J|A|C|S
ARTICLES
Published on Web 03/13/2002

Ru(II) and Os(II) Nucleosides and Oligonucleotides: Synthesis and Properties

Dennis J. Hurley and Yitzhak Tor*

Contribution from the Department of Chemistry and Biochemistry, University of California, San Diego, La Jolla, California 92093-0358

Received October 9, 2001. Revised Manuscript Received January 3, 2002

Abstract: A general and versatile method for the site-specific incorporation of polypyridine Ru^{II} and Os^{II} complexes into DNA oligonucleotides using solid-phase phosphoramidite chemistry is reported. Novel nucleosides containing a $[(bpy)_2M(3\text{-ethynyl-}1,10\text{-phenanthroline})]^{2+}$ (M = Ru, Os) metal center covalently attached to the 5-position in 2′-deoxyuridine are synthesized, and their electrochemical as well as photophysical properties are studied. The Ru^{II} nucleoside exhibits a rather long-lived excited state in phosphate buffer pH 7.0 ($\tau = 1.08\ \mu s$) associated with a relatively high emission quantum efficiency ($\phi = 0.051$). The solvent dependence of the absorption and emission spectra is consistent with an emissive MLCT state where charge localization takes place on the extended heterocycle-linked phenanthroline. In contrast, the Os^{II}-containing nucleoside is quite nonemissive in aqueous environment ($\tau = 0.027\ \mu s$, $\phi = 1 \times 10^{-4}$). The metal-containing nucleosides are converted into their phosphoramidites and are utilized for the high-yield preparation of modified oligonucleotides. The novel oligonucleotides, characterized by absorption and emission spectroscopy, enzymatic digestion, and electrophoresis, form stable duplexes. Circular dichroism spectra confirm that the global conformation of the double helix is not altered by the presence of these polypyridyl complexes in the major groove. Metal-containing phosphoramidites with predetermined absolute configuration at the octahedral coordination center are synthesized and utilized for the synthesis of diasteromerically pure metal-containing DNA oligonucleotides. Emission spectroscopy suggests a higher protection of the Δ metal center from the bulk solvent and better accommodation within the major groove.

Introduction

Oligonucleotides containing photo- and redox-active transition metal complexes have become a unique tool for studying photophysical processes in nucleic acids,[1,2] as well as for the assembly of DNA hybridization probes and sensors.[3] The incorporation of coordination compounds into oligonucleotides has been traditionally accomplished by a postsynthetic metal complexation of a chelate-containing oligonucleotide,[3c,4] or by conjugation of a functionalized oligonucleotide with a suitably activated metal complex.[1,5] Most approaches facilitate the incorporation of coordination complexes at the oligo's termini, while internal modification remains a challenge.[6,7] A general methodology for the incorporation of metal centers at any

(1) For selected examples, see Murphy, C. J.; Arkin, M. R.; Jenkins, Y.; Ghatlia, N. D.; Bossmann, S. H.; Turro, N. J.; Barton, J. K. *Science* **1993**, *262*, 1025−1029. Meade, T. J.; Kayyem, J. F. *Angew. Chem., Int. Ed. Engl.* **1995**, *34*, 352−354. Dandliker, P. J.; Holmlin, R. E.; Barton, J. K. *Science* **1997**, *275*, 1465−1468. Holmlin, R. E.; Tong, R. T.; Barton, J. K. *J. Am. Chem. Soc.* **1998**, *120*, 9724−9725. Ortmans, I.; Content, S.; Boutonnet, N.; Kirsch-De Mesmaeker, A.; Bannwarth, W.; Constant, J.-F.; Defrancq, E.; Lhomme, J. *Chem. Eur. J.* **1999**, *5*, 2712−2721. Stemp, E. D. A.; Holmlin, R. E.; Barton, J. K. *Inorg. Chim. Acta* **2000**, *297*, 88−97. Schiemann, O.; Turro, N. J.; Barton, J. K. *J. Phys. Chem. B* **2000**, *104*, 7214−7220. Williams, T. T.; Odom, D. T.; Barton, J. K. *J. Am. Chem. Soc.* **2000**, *122*, 9048−9049.

(2) For overview articles, see Netzel, T. L. *J. Chem. Educ.* **1997**, *74*, 646−651. Diederichsen, U. *Angew. Chem., Int. Ed. Engl.* **1997**, *36*, 2317−2319. Holmlin, R. E.; Dandliker, P. J.; Barton, J. K. *Angew. Chem., Int. Ed. Engl.* **1997**, *36*, 2714−1730. Netzel, T. L. *J. Biol. Inorg. Chem.* **1998**, *3*, 210−214. Erkkila, K. E.; Odom, D. T.; Barton, J. K. *Chem. Rev.* **1999**, *99*, 2777−2795. Grinstaff, M. W. *Angew. Chem., Int. Ed.* **1999**, *38*, 3629−3635. Núñez, M. E.; Barton, J. K. *Curr. Opin. Chem. Biol.* **2000**, *4*, 199−206.

(3) (a) Bannwarth, W.; Schmidt, D.; Stallard, R. L.; Hornung, C.; Knorr, R.; Müller, F. *Helv. Chem. Acta* **1988**, *71*, 2085−2099. (b) Bannwarth, W.; Schmidt, D. *Tetrahedron Lett.* **1989**, *30*, 1513−1516. (c) Telser, J.; Cruickshank, K. A.; Schanze, K. S.; Netzel, T. L. *J. Am. Chem. Soc.* **1989**, *111*, 7221−7226. (d) Bannwarth, W.; Pfleiderer, W.; Müller, F. *Helv. Chem. Acta*, **1991**, *74*, 1991−1999.

(4) Bashkin, J. K.; Frolova, E. I.; Sampath, U. *J. Am. Chem. Soc.* **1994**, *116*, 5981−5982. Matsumura, K.; Endo, M.; Komiyama, M. *J. Chem. Soc., Chem. Commun.* **1994**, 2019−2020. Chen, C.-H. B.; Sigman, D. S. *J. Am. Chem. Soc.* **1988**, *110*, 6570−6572.

(5) Magda, D.; Miller, R. A.; Sessler, J. L.; Iverson, B. L. *J. Am. Chem. Soc.* **1994**, *116*, 7439−7440. Hall, J.; Hüsken, D.; Pieles, U.; Moser, H. E.; Häner, R. *Chem. Biol.* **1994**, *1*, 185−190. Hall, J.; Hüsken, D.; Häner, R. *Nucleic Acids Res.* **1996**, *24*, 3522−3526.

(6) For approaches utilizing metal-containing phosphoramidites or H-phosphonates, see Manchanda, R.; Dunham, S. U.; Lippard, S. J. *J. Am. Chem. Soc.* **1996**, *118*, 5144−5145. Schlipe, J.; Berghoff, U.; Lippert, B.; Cech, D. *Angew. Chem., Int. Ed. Engl.* **1996**, *35*, 646−648. Music, R. C.; Herrlien, M. K.; Mirkin, C. A.; Letsinger, R. L. *Chem. Commun.* **1996**, 555−557. Meggers, E.; Kusch, D.; Giese, B. *Helv. Chim. Acta* **1997**, *80*, 640−652. Magda, D.; Crofts, S.; Lin, A.; Miles, D.; Wright, M.; Sessler, J. L. *J. Am. Chem. Soc.* **1997**, *119*, 2293−2294. Lewis, F. D.; Helvoigt, S. A.; Letsinger, R. L. *Chem. Commun.* **1999**, 327−328. Wiederholt, K.; McLaughlin, L. W. *Nucleic Acids Res.* **1999**, *27*, 2487−2493. For a photoaddition of Ru^{II} complex to DNA, see Jacquet, L.; Davis, R. J. H.; Kirsch-De Mesmaeker, A.; Kelly, J. M. *J. Am. Chem. Soc.* **1997**, *119*, 11763−11768. For an overview article, see Beilstein, A. E.; Tierney, M. T.; Grinstaff, M. W. *Comments Inorg. Chem.* **2000**, *22*, 105−127.

(7) Following the publication of our preliminary communication (ref 8), a nonconjugated Ru^{II}-containing phosphoramidite (Khan, S. I.; Beilstein, A. E.; Grinstaff, M. W. *Inorg. Chem.* **1999**, 38, 418−419) and solid-support modifications (Khan, S. I.; Grinstaff, M. W. *J. Am. Chem. Soc.* **1999**, *121*, 4704−4705) have been reported.

10.1021/ja0123103 CCC: $22.00

position along the DNA sequence using automated DNA synthesizers is highly desirable. This capability is particularly important when the systematic study of energy- and electron-transfer processes in DNA is concerned: changing the distance between the termini requires the synthesis of oligonucleotides of variable lengths, while varying the internal positioning of metal probes within a single DNA template will allow to methodically study distance-dependency without sequence perturbations.

A systematic approach to the modification of DNA with photo- and redox-active metal centers needs to fulfill the following requirements: (a) generality − the incorporation of the metal complexes at any position along the DNA duplex should be possible; (b) structural stability − the modification should ensure minimal structural perturbation of the DNA duplex; (c) placement − the complexes have to be directly connected to the stacked heterocyclic bases; (d) versatility and tunability − a family of novel bases with a range of redox potentials and spectral characteristics, as well as tunable electronic communication with the heterocycle, should be accessible; and (e) simplicity − the building blocks should be synthetically accessible and compatible with standard solid-phase DNA synthesis.

In a preliminary account, we reported the first solid-phase controlled synthesis of Ru^{II}- and Os^{II}-containing oligonucleotides.[8] Our approach involves the synthesis of metal-containing phosphoramidites and their sequence-specific incorporation into oligonucleotides using standard automated phosphoramidite chemistry. In this paper, we outline the design criteria and the experimental details involved in preparing, characterizing, and studying metal-containing oligonucleotides. We describe the synthesis and characterization of Ru^{II}- and Os^{II}-containing nucleosides, as well as their redox and photophysical characteristics. We discuss the preparation and purification of the modified phosphoramidites and their facile incorporation into metal-containing DNA oligonucleotides. The analysis of the novel oligonucleotides is outlined in detail, together with their photophysical characteristics. We report, for the first time, the synthesis of metal-containing phosphoramidites with predetermined absolute configuration at the octahedral coordination center, and their utilization for the synthesis of diasteromerically pure metal-containing DNA oligonucleotides. The hybridization and luminescence properties of the metal-modified oligonucleotides are discussed. These uniquely modified oligonucleotides form stable DNA duplexes and are valuable tools for the study of photophysical processes in nucleic acids.

Results and Discussion

Design Criteria. Several major factors were taken into consideration in designing our first-generation metal-containing nucleosides suitable for automated DNA synthesis: (1) the base modification position, (2) the nature of the linking group, (3) the kinetic stability of the metal centers and their compatibility with standard conditions of automated DNA synthesis, as well as (4) synthetic accessibility and versatility. We have chosen to covalently attach Ru^{II} and Os^{II} polypyridine complexes to the 5-position of 2′-deoxyuridine (Figure 1). A modification at this position is projected into the major groove of the double helix and is likely to have little impact on the stability of duplex

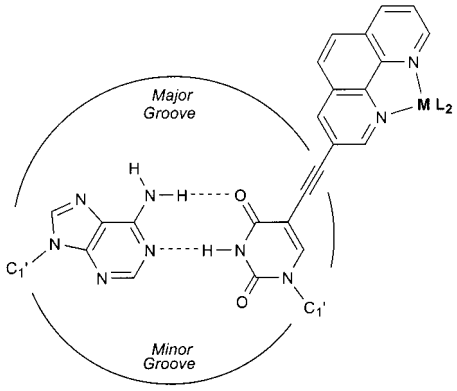

Figure 1. Base-paired conjugated metal-containing deoxyuridine nucleosides point toward the major groove of the double-helix. Note the potential versatility in coordinated metal ions and co-ligands.

DNA.[9] The rigid ethynyl linker ensures that the metal complex does not back-intercalate into the duplex and produces substantial electron delocalization, allowing for electronic communication between the base-pairing heterocycle and the metal chelator.[10] Polypyridine complexes of Ru^{II} and Os^{II} were selected due to their chemical stability, and favorable redox and photophysical characteristics.[11] The availability of 5-halogenated pyrimidines together with numerous cross coupling methodologies provides multiple synthetic routes to novel modified nucleobases.

Synthesis of Metal-Containing Nucleosides. We prepared the metal-containing nucleosides **5a** and **5b**, employing functionalized coordination compounds as synthetic building blocks.[12,13] The approach entails the synthesis of 5-ethynyldeoxyuridine **2**, a known modified nucleoside prepared from the commercially available 5-iododeoxyuridine **1**,[14,15] followed by a Sonogashira cross-coupling reaction with coordination complexes $[(bpy)_2M(3\text{-bromo-}1,10\text{-phenanthroline})]^{2+}(PF_6^-)_2$.[12,13] Thus, **2** was cross-coupled to **4a** and **4b** in the presence of $(dppf)PdCl_2 \cdot CH_2Cl_2$, CuI, and DMF/$Et_3N$ to afford the Ru^{II}- and Os^{II}-containing nucleosides **5a** and **5b**, respectively, in high yields (Scheme 1).

The high reactivity of the functionalized metal complexes **4a** and **4b** in cross-coupling reactions[12,13] enabled us to similarly modify 5′-(4,4′-dimethoxytrityl)-protected nucleosides. Thus, **2** is first treated with 4,4′-dimethoxytrityl chloride (DMT-Cl) in the presence of DMAP to provide the DMT-protected nucleoside **3**. Cross coupling with **4a** and **4b** provides the 5′-protected metal-containing nucleosides **6a** and **6b**, respectively.[16] Phos-

(8) Hurley, D. J.; Tor, Y. *J. Am. Chem. Soc.* **1998**, *120*, 2194−2195.

(9) Ethynyl-linked substitutions at the 5 positions are particularly favored; see Ahmadian, M.; Zhang, P.; Bergstrom, D. E. *Nucleic Acids Res.* **1998**, *26*, 3127−3135.

(10) Tzalis, D.; Tor, Y. *Tetrahedron Lett.* **1995**, *36*, 6017−6020.

(11) (a) Juris, A.; Balzani, V.; Barigelletti, F.; Campagna, S.; Belser, P.; Von Zelewsky, A. *Coord. Chem. Rev.* **1988**, *85*, 85−277. (b) Sauvage, J.-P.; Collin, J.-P.; Chambron, J.-C.; Guillerez, S.; Coudret, C.; Balzani, V.; Barigelletti, F.; De Cola L.; Flamigni, L. *Chem. Rev.* **1994**, *94*, 993−1019. (d) Balzani, V.; Juris, A.; Venturi, M.; Campagna, S.; Serroni, S. *Chem. Rev.* **1996**, *96*, 659−833. (e) Barigelletti, F.; Flamigni, L.; Collin, J.-P.; Sauvage, J.-P. *Chem. Commun.* **1997**, 333−338.

(12) Tzalis, D.; Tor, Y. *Chem. Commun.* **1996**, 1043−1044.

(13) Connors, P. J., Jr.; Tzalis, D.; Dunnick, A. L.; Tor, Y. *Inorg. Chem.* **1998**, *37*, 1121−1123.

(14) Robins, M. J.; Barr, P. J. *J. Org. Chem*. **1983**, *48*, 1854−1862.

(15) Hashimoto, H.; Nelson, M. G.; Switzer, C. *J. Am. Chem. Soc.* **1993**, *115*, 7128−7138.

(16) Attempts to protect the 5′-hydroxyl in the metalated nucleosides **5a** and **5b** as the DMT derivatives were unsuccessful. It is likely that the bulky polypyridine complexes interfere with this reaction. See also Supporting Information for additional evidence for the interaction between the 5′-DMT group and the metal center at the 5 position.

Scheme 1. Synthesis of Phosphoramidites **7a** and **7b**[a,b]

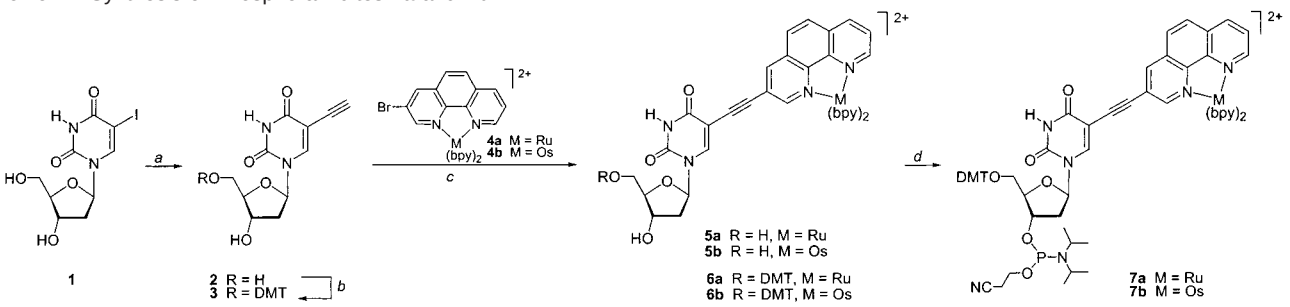

[a] Reagents: (a) i. $(CF_3CO)_2O$; ii. $Me_3Si-C\equiv CH$, $(Ph_3P)_4Pd$, CuI, DMF, Et_3N, 95−98%; iii. K_2CO_3, MeOH, 75−92%; (b) 4,4′-dimethoxytrityl chloride (DMT-Cl), DMAP, pyridine, Et_3N, 92%; (c) $(dppf)PdCl_2 \cdot CH_2Cl_2$, CuI, DMF, Et_3N, 72−84%; (d) $(iPr_2N)_2POCH_2CH_2CN$, (1*H*)-tetrazole, CH_3CN, 75−92%. [b] All metal-modified nucleosides were isolated as their PF_6^- salts.

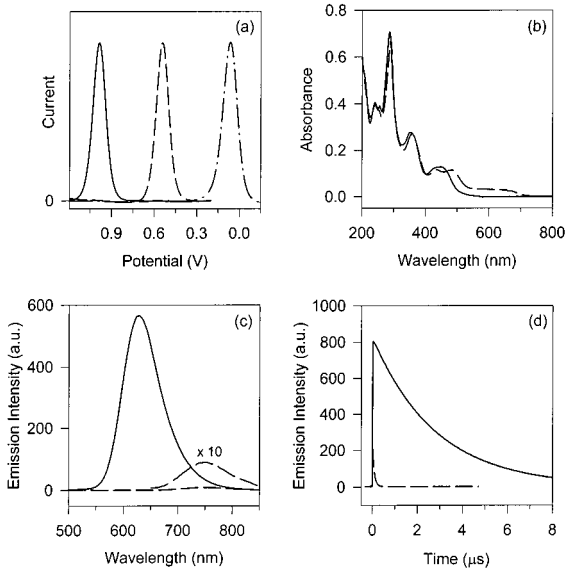

Figure 2. Electrochemical and photophysical characteristics of metalated nucleosides. (a) Square-wave voltammograms of **5a** (solid line) and **5b** (dashed line) shown next to ferrocene (−·−·). All taken in degassed acetonitrile solution containing 0.1 M $[n\text{-}Bu_4N^+][PF_6^-]$ vs Ag/Ag^+. (b) UV−Vis absorption spectra of **5a** (solid line) and **5b** (dashed line) in acetonitrile. (c) Steady-state emission spectra of **5a** (solid line) and **5b** (dashed line) in deoxygenated acetonitrile. (d) Time-resolved luminescence decay of **5a** (solid line) and **5b** (dashed line) in acetonitrile.

phitylation of the protected nucleosides with 2-cyanoethyl-*N*,*N*,*N*′,*N*′-tetraisopropylphosphorodiamidite in the presence of (1*H*)-tetrazole provided the corresponding metal-containing phosphoramidites **7a** and **7b** (Scheme 1). These phosphoramidites have been carefully purified by flash chromatography over basic alumina using acetonitrile−water mixtures containing saturated KPF_6 (see experimental part). As discussed below, high purity of the phosphoramidites was found to be critical for ensuring high coupling efficiency during oligonucleotide synthesis. These sensitive building blocks were therefore thoroughly characterized by ^1H, and ^{31}P NMR together with ESI mass spectrometry.

Redox and Photophysical Properties of Metal-Containing Nucleosides. In addition to the routine analytical characterization of the new metal modified nucleosides (see experimental part), we have examined their redox and photophysical properties. As illustrated in Figure 2a, square wave voltammetry in acetonitrile shows a well-defined $M^{2+/3+}$ wave at ca. +1.0 and +0.56 V (vs Ag/Ag^+) for nucleosides **5a** and **5b**, respectively.[17] For calibration, the ferrocene/ferrocinium (Fc/Fc^+) couple, measured under the same conditions, is also shown (+85 mV vs Ag/Ag^+). The values obtained for the metalated nucleosides are in good agreement with prototypical Ru^{II} and Os^{II} polypyridine complexes.[11,13]

Table 1. Redox and Photophysical Properties of Metal-Containing Nucleosides **5a** and **5b**[a]

comp	$E_{1/2}$[b] ($M^{3+/2+}$)	UV−Vis[c]	λ_{em}[d]	Φ_{em}[e]	τ[f]
5a	0.993	242 (4.0), 256 (3.9), 286 (6.9), 352 (2.6), 450 (1.3)	629 [633]	0.137 [0.051]	2.78 [1.08]
5b	0.560	242 (3.8), 254 (3.6), 290 (6.4), 358 (2.6), 436 (1.1), 484 (1.1)[g]	749 [754]	0.0003 [0.0001]	0.078 [0.027]

[a] Measurements were performed with 1×10^{-5} M deoxygenated acetonitrile solutions at room temperature. λ_{em}, Φ_{em}, and τ values in brackets are for deoxygenated aqueous solutions. [b] Redox potentials in V as measured in acetonitrile vs Ag/Ag^+; $E_{1/2} = 0.085$ V for Fc/Fc^+ under these conditions. [c] In acetonitrile. Absorption maxima are given in nm and extinction coefficients ($\epsilon \times 10^{-4}$ in parentheses) in M^{-1} cm^{-1}. In water, the phenanthroline absorption bands shift from 352 (2.6) to 346 (3.2) for **5a** and from 358 (2.6) to 352 (2.8) for **5b**. [d] Excitation at 450 nm. λ_{em} reported in nm. [e] MLCT emission quantum yields were calculated from the integrated spectra relative to $Ru(bpy)_3$ in H_2O ($\Phi = 0.042$). [f] Lifetimes are reported in μs. Decays were monitored at the λ_{em} for each compound. Estimated error is 3%. [g] Broad absorption tailing to >600 nm.

The absorption and emission characteristics of the Ru^{II} and Os^{II} nucleosides are shown in Figure 2b−d, and the data are summarized in Table 1. Both nucleosides exhibit intense $\pi-\pi^*$ transitions of the aromatic diimine ligands at 280 nm, a lower energy transition, assigned to the extended phenanthroline at 350 nm,[12,13] and typical metal-to-ligand charge-transfer (MLCT) transitions in the visible region (ca. 450 nm for Ru^{II}, 440 and 500 nm for Os^{II}). Excitation of an acetonitrile solution of **5a** at 460 nm leads to an intense red emission centered at 630 nm (Figure 2c). Using the method reported by Crosby,[18] the quantum efficiency of the Ru-based emission in acetonitrile was determined to be 0.137. This value is twice as high as compared to $[Ru(bpy)_3]^{2+}$ (0.062).[19] The higher luminescence efficiency is also manifested in the relatively long-lived excited state of **5a** ($\tau = 2.78$ μs) when compared to $[Ru(bpy)_3]^{2+}$ ($\tau = 0.87$ μs).[20] These differences are likely to result from the lower symmetry of the metal complex and extended conjugation of the phenanthroline ligand in **5a**. In contrast, the Os^{II}-containing nucleosides **5b** is quite nonemissive, giving rise to a weak

(17) Cyclic voltammetry measurements under identical conditions show reversible, one-electron $M^{2+/3+}$ waves for the metal-containing nucleosides **5a** and **5b** ($\Delta E_p \cong 60-90$ mV, $i_a \cong i_c$).
(18) Demas, J. N.; Crosby, G. A. *J. Phys. Chem.* **1971**, *75*, 991−1024.
(19) Casper, J. V.; Meyer, T. J. *J. Am. Chem. Soc.* **1983**, *105*, 5583−5590.
(20) Elfring, W. H., Jr.; Crosby, G. A. *J. Am. Chem. Soc.* **1981**, *103*, 2683−2687. Kaizu, Y.; Ohta, H.; Kobayashi, K.; Kobayashi, H.; Takuma, K.; Matsuo, T. *J. Photochem.* **1985**, *30*, 93−103.

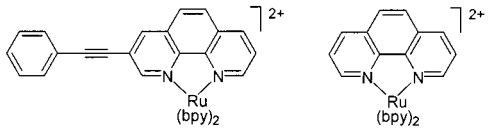

8 **9**

Figure 3. Model compounds utilized for solvatochromism studies.

Table 2. Solvent-Dependent Absorption and Emission Maxima[a]

	5a			8			9		
solvent	λ_{max} (nm)	ϵ^b	$\lambda_{em}{}^c$ (nm)	λ_{max} (nm)	ϵ^b	$\lambda_{em}{}^c$ (nm)	λ_{max} (nm)	ϵ^b	$\lambda_{em}{}^c$ (nm)
H_2O	344	3.2	633	330	3.0	631	264	5.1	607
MeOH	354	2.7	624	342	2.7	623	266	4.9	603
iPrOH	358	2.4	621	344	2.4	619	266	4.6	598
CH_3CN	354	2.6	624	332	2.7	629	266	4.2	607
CH_2Cl_2	360	2.0	607	348	2.6	609	268	5.1	598

[a] All measurements were performed on nondeoxygenated 1×10^{-5} M solutions. [b] Extinction coefficients are of the phenanthroline $\pi-\pi^*$ absorption band and are reported in $10^{-4} \times M^{-1}\ cm^{-1}$. [c] Excitation at the MLCT band (450 nm).

emission centered at 750 nm with emission quantum efficiency of ca. 3×10^{-4}, and a very short excited-state lifetime ($\tau = 0.078\ \mu s$) in deoxygenated acetonitrile (Figure 2d and Table 1).[21] As anticipated, both nucleosides are less emissive in aqueous solutions, with emission quantum efficiencies of 0.051 and $<1 \times 10^{-4}$ for the Ru^{II} and Os^{II} nucleosides, respectively. This is also reflected in shorter excited lifetimes in degassed buffered solution. The excited states for both the free Ru^{II} and Os^{II} nucleoside are characterized by single exponential decays, regardless of the solvent employed.

Extending the conjugation of the rigid 1,10-phenanthroline at the 3 and 8 positions has a substantial effect on the electronic properties of the free ligands as well as the resulting transition metal complexes.[12,22] The electronic delocalization offered by the aryl-ethynyl substitution at these positions results in red-shifted ligand-centered transitions and emission bands, as well as increased sensitivity to the environment when compared to unmodified phenanthroline ligands or phenanthroline-containing complexes.[22] To learn about the excited-state properties of the metal-containing nucleosides, the absorption and emission spectra of the Ru^{II}-containing nucleoside were studied in different solvents, ranging from water to dichloromethane. For comparison, the spectra of $[(bpy)_2Ru(3\text{-phenylethynyl-phen})]^{2+}$ **8** and $[(bpy)_2Ru(phen)]^{2+}$ **9** were also recorded. Complex **8** has a similar extended ring structure as found in the Ru^{II} nucleoside **5a**, but lacks the hydrogen-bonding capability and 2′-deoxyribose moiety of the nucleoside, and derivative **9** lacks any extended ligands (see Figure 3 for structures).

In the absorption spectra, solvatochromism is primarily manifested in changes in intensity and absorption maxima of the band around 350 nm, which is attributed to the $\pi-\pi^*$ transition of the extended phenanthroline ligand (Table 2).[22,23] In the nucleoside **5a**, this transition is red-shifted from 344 nm in water to 360 nm in dichloromethane, while the MLCT and the bipyridine $\pi-\pi^*$ remain unaffected. Associated with this bathochromic shift in the absorption maxima upon decreasing solvent polarity is a concomitant hypochromic effect. The phenanthroline's $\pi-\pi^*$ extinction coefficient decreases from 3.2×10^4 in water to $2.0 \times 10^4\ M^{-1}\ cm^{-1}$ in dichloromethane. Complex **8** shows very similar behavior, and the absorption band is red shifted from 330 nm in water to 348 nm in dichloromethane. This transition also suffers a hypochromic effect, albeit to a lower extent (Table 2). In contrast, the parent complex **9** that lacks any extended conjugation shows very little solvatochromic behavior with the higher energy phenanthroline $\pi-\pi^*$ transition shifting from 264 nm in water to 268 nm in dichloromethane.

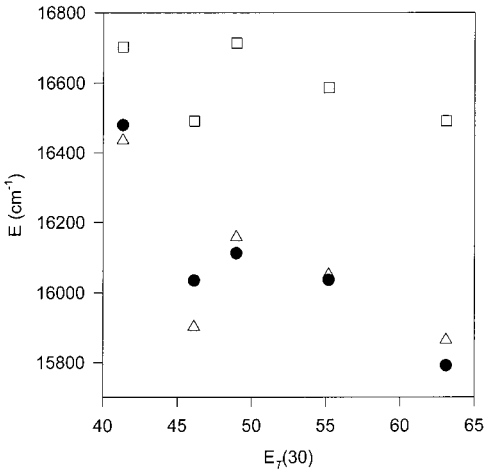

Figure 4. Solvent-dependent emission energies of nucleoside **5a** (●) and reference compounds **8** (△) and **9** (□) plotted against the experimentally determined $E_T(30)$ values.

In Ru^{II}-polypyridyl complexes, it is typically the low-lying MLCT excited state that is emissive.[11a] Figure 4 shows a plot of the emission energy of **5a**, **8**, and **9** against the solvent polarity $E_T(30)$ value. Both the metal-containing nucleoside **5a** and the extended complex **8** exhibit significant positive solvatochromism, where their emission maxima are red-shifted with increasing solvent polarity, from below 610 nm in dichloromethane to above 630 nm in water. In contrast, a minimal solvatochromic effect on the emission maxima is observed for the reference unsubstituted complex **9**.

Solvatochromism results from the differential solvation of the ground and excited states, and is intimately associated with changes in the molecular dipole moment upon electronic excitation. The significant hypsochromic shift observed for the ground-state absorption spectra of nucleoside **5a** and the analogous complex **8** upon increasing solvent polarity, together with the corresponding bathochromic shift observed in the emission spectra, suggest destabilization of the ground state and stabilization of the emissive excited state. This contrasts the relatively low sensitivity of the absorption and emission spectra of the unsubstituted $[(bpy)_2Ru(phen)]^{2+}$ **9** to solvent polarity. Taken together, these observations imply that the extended complexes undergo significant changes in dipole moment upon electronic excitation. We therefore suggest that the emissive charge separated MLCT excited state in complexes **5a** and **8** is not delocalized over all polypyridyl ligands, but rather the promoted electron is mainly localized on the extended phenanthroline ligand.[24,25]

(21) As with the Ru^{II} nucleoside **5a**, the excited-state lifetime of the Os^{II}-containing nucleoside **5b** (Table 1) is also longer lived than the lifetime of the "parent" $Os(bpy)_3$ ($\tau = 0.060$ and $0.019\ \mu s$ in acetonitrile and water, respectively). See Kober, E. M.; Caspar, J. V.; Lumpkin, R. S.; Meyer, T. J. *J. Phys. Chem.* **1986**, *90*, 3722−3734; Creutz, C.; Chou, M.; Netzel, T. L.; Okumura, M.; Sutin, N. *J. Am. Chem. Soc.* **1980**, *102*, 1309−1319.

(22) Joshi, H. S.; Jamshidi, R.; Tor, Y. *Angew. Chem. Int. Ed.* **1999**, *38*, 2721−2725.

(23) See Supporting Information for additional experimental details.

To characterize the excited-state redox potential of the Ru^{II} nucleoside **5a**, its ground-state reduction waves were recorded next to that of $[(bpy)_2Ru(phen)]^{2+}$ **9**. The Ru^{II} nucleoside **5a** shows a reduction wave at −1.12 V, and is easier to reduce than **9** which shows a corresponding wave at −1.28 V (vs SCE). On the basis of these potentials and the E^{0-0} transition energies (calculated at the 5% onset of emission), we have determined the excited-state redox potentials in DMF at room temperature.[23,26] Nucleoside **5a** is thus slightly more oxidizing in the excited state ($^*E_{red} = +1.05$ V vs SCE) than the unsubstituted complex **9** ($^*E_{red} = +1.03$ V vs SCE).[27]

Oligonucleotide Synthesis and Purification. The novel phosphoramidites **7a** and **7b** can be employed for the synthesis of metal-containing oligonucleotides using the standard solid-phase phosphoramidite DNA synthesis conditions. To control the amount of reagents and reaction time, the coupling of the modified base was performed manually (see experimental part). It is important to note that the coupling efficiency of the metal-containing phosphoramidites during DNA synthesis has been found to be critically influenced by their purity and the amount of (1*H*)-tetrazole utilized for their activation. When the highly pure phosphoramidites **7a** and **7b** were coupled for 5 min in the presence of 0.5 M (1*H*)-tetrazole, reaction efficiencies were greater than 90%.[28] Lower (1*H*)-tetrazole concentrations and slight impurities would substantially decrease the reaction efficiency to 50% or lower.

Numerous metal-containing oligonucleotides varying in length, modified base position as well as composition have been synthesized in good yields using the novel metal-containing phosphoramidites **7a** and **7b** (Figure 5). Removal of the completed oligonucleotides from the solid support using concentrated ammonium hydroxide was followed by incubation at 55 °C for 8−12 h to afford the crude oligonucleotides. The metal-containing oligonucleotides were purified by denaturing polyacrylamide gel electrophoresis and semipreparative HPLC. HPLC analysis of the gel-purified oligonucleotides indicated 85−90% purity, which was satisfactory for many of the studies reported below.[23] Higher purity level (>95%) could be reached by HPLC purification of a fully deprotected oligonucleotide containing a 5′-DMT group. Acidic deprotection, followed by an additional semipreparative HPLC purification, affords analytically pure metal-containing oligonucleotides (see Experimental Section).

Oligonucleotide Characterization. The synthesis of internally modified oligonucleotides (e.g., **11**, **15**) requires the exposure of the metal-containing nucleotide to multiple coupling, capping, and deprotection steps. The modified oligonucleotides have therefore been carefully characterized. Figure 6 shows an analytical denaturing polyacrylamide gel comparing several representative metal-containing 20-mer oligonucleotides to their corresponding unmodified counterpart. Due to the increased mass and reduced overall charge, the electrophoretic mobility of the metal-containing oligonucleotides **15**−**17** is slower than the corresponding unmodified oligonucleotide **14**. Among the metal-containing oligonucleotides, the internally modified DNA oligos migrate slightly slower than the oligonucleotides with a metal at the 5′-end. Oligonucleotides containing two metal centers (e.g., **18**) exhibit twice the retardation when compared to a singly modified oligonucleotides **15** or **16**.

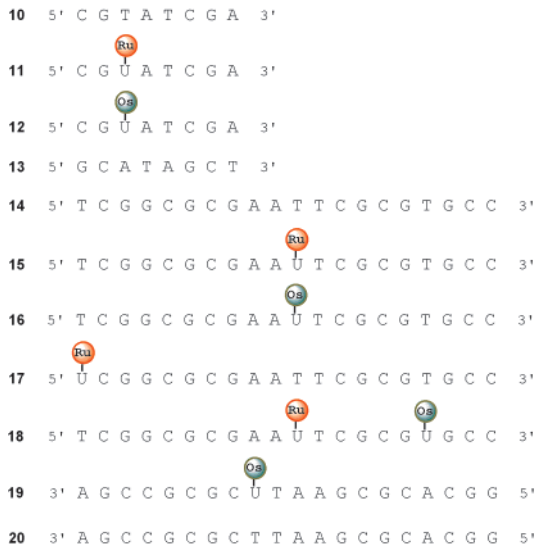

Figure 5. Sequences of oligonucleotides synthesized. The modified bases are denoted as orange circles for **5a** and olive-colored circles for **5b**.

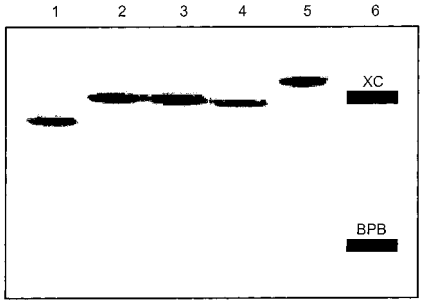

Figure 6. Denaturing 20% polyacrylamide gel used for the analysis of metal-containing oligonucleotides. Lane 1 − control 20-mer **14**; lane 2 − Ru^{II}-containing oligonucleotide **15**; lane 3 − Os^{II}-containing oligonucleotide **16**; lane 4 − Ru^{II}-containing oligonucleotide **17**; lane 5 − dimetalated Ru^{II}- and Os^{II}-containing oligonucleotide **18**; lane 6 − rectangles show the relative location of the dye markers xylene cyanol and bromophenol blue. Oligonucleotides were visualized using Stains-all.

Enzymatic digestion reactions followed by HPLC analysis of the nucleoside mixture were routinely employed to verify the presence of the intact metal-containing nucleosides in the modified oligonucleotides.[23] Initially, a mixture of snake venom phosphodiesterase and alkaline phosphatase was employed. HPLC analysis indicated incomplete digestion, corresponding to phosphodiester hydrolysis and dephosphorylation of the natural nucleotides 3′-to the modification position. This was confirmed by an independent digestion of an unmodified oligonucleotide corresponding to the truncated sequence 3′ to the metal-containing nucleoside. This may have resulted from the inability of the phosphodiesterase, an exonuclease digesting from the 3′-end of an oligonucleotide, to proceed past the bulky

(24) McCusker has recently demonstrated that even in $Ru(bpy)_3$ the rapid initial delocalization of the excited state is followed by localization of the transferred charge into a single ligand. See Yeh, A. T.; Shank, C. V.; McCusker, J. K. *Science* **2000**, *289*, 935−938.

(25) Additional support is obtained from transient absorption spectra taken between 320 and 570 nm that show bleaching of the band at 350 nm, associated with the ground-state absorption band of the conjugated phenanthroline (see Figure S-2 in Supporting Information).

(26) Square wave voltammetry was measured in DMF containing 0.1 M $[n\text{-}Bu_4N^+][PF_6^-]$ as supporting electrolyte. DMF was used as it offers a wider potential window at negative potentials that are required for the clear recording of the reduction waves. Consequently, the emission spectra were also taken in DMF.

(27) The value we determine for **9** is different than the value reported by Meyer ($^*E_{red} = +0.78$ V vs SCE).[19] Note, however, that Meyer's value was determined by recording emission at 77 K in EtOH/MeOH glass.

(28) Coupling efficiencies were determined by quantifying the amount of trityl cation release after each coupling step (see experimental part).

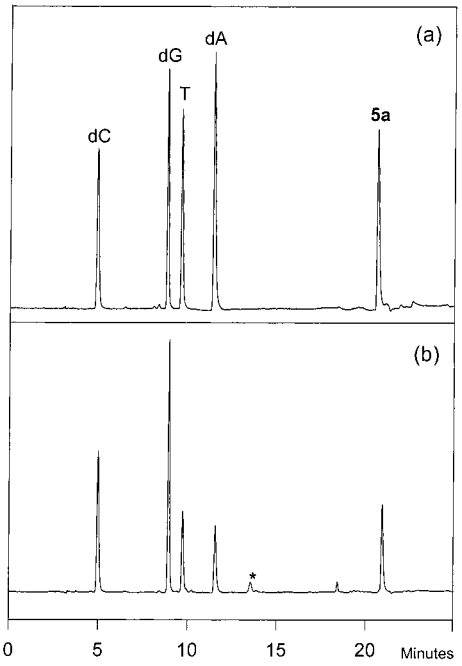

Figure 7. HPLC chromatograms of an enzymatic digestion reaction of a Ru^{II}-containing oligonucleotide **15** (b) vs a mixture of nucleoside standards (a). Chromatograms were monitored at 260 nm. Impurities found in a blank digestion mixture are marked with an asterisk.

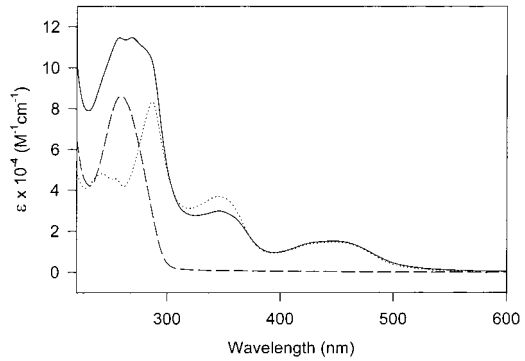

Figure 8. UV−Vis absorption spectra of a Ru^{II}-containing oligonucleotide **11** (solid line), the corresponding unmodified oligonucleotide **10** (dashed line), and the Ru^{II}-containing nucleoside **5a** (dotted line) in 10 mM phosphate buffer, pH 7.0, and 100 mM NaCl.

base modification. To overcome this difficulty, we added nuclease P1, an endonuclease, to our enzyme mixture. Thus, incubation of the metal-modified oligonucleotides with snake venom phosphodiesterase, alkaline phosphatase, and nuclease P1 at 37 °C for 6 to 12 h, resulted in complete phosphodiester hydrolysis and dephophorylation to yield a mixture of the natural and modified nucleosides. Figure 7 depicts a reversed-phase HPLC analysis of the nucleoside mixture obtained by digesting oligonucleotide **15**, a 20-mer containing a single modification site. A comparison to the HPLC trace obtained for a standard mixture of the natural and synthetic nucleosides verifies the presence and correct stoichiometry of the intact metal-containing nucleoside **5a**.[23]

Figure 8 compares the absorption spectrum of a metal containing oligonucleotide to that of an unmodified oligonucleotide of the same length and to the parent metal-containing nucleoside. The spectrum of **11**, a Ru^{II}-containing 8-mer, exhibits the typical transitions of the heterocyclic DNA bases around 260 nm. Additional bands around 300, 350, and 450 nm are attributed to the bipyridine $\pi-\pi^*$, phenanthroline $\pi-\pi^*$, and the MLCT transition, respectively. To a first approximation, this spectrum appears as a superposition of the absorption spectra of the nucleoside and the unmodified oligonucleotide. However, a slight red shift and a diminished intensity of the phenanthroline $\pi-\pi^*$ band in the modified oligonucleotide **11** is observed. These changes are in accord with the spectral features of the parent nucleoside **5a** in solvents that less polar than water. This suggests that even in a single-stranded oligonucleotide, stacking interactions with neighboring heterocycles may shield the coordinated phenanthroline ligand from the aqueous bulk solvent.

Table 3. Thermal Melting Temperatures (T_m) of Unmodified and Metal-Containing DNA Duplexes[a]

DNA duplex	T_m (°C)	DNA duplex	T_m (°C)
10·13	44	**16·20**	75
11·13	40	**17·20**	79
12·13	40	**18·20**	70
14·20	78	**15·19**	75
15·20	75	**17·19**	78

[a] T_m values were determined from the first derivative of the melting curve monitored at 260 nm. Solutions were 2 μM duplex in 100 mM NaCl, 10 mM phosphate buffer pH 7.0. Estimated error is ± 0.5 °C.

Oligonucleotide Hybridization. Metal-containing oligonucleotides have been hybridized with their unmodified or metal-containing complements using standard denaturation-reannealing cycles. An equimolar buffered solution of the two single-stranded oligonucleotides is heated to 90 °C and then cooled slowly to room temperature. Thermal denaturation studies of the annealed duplexes done between 20 and 95 °C were used to evaluate the relative stability of the metal-modified duplexes with respect to their unmodified counterparts. The data are summarized in Table 3.[23] The presence of a metal-containing nucleoside in the middle of the G-rich duplex **15·20** slightly destabilizes the duplex when compared to **14·20**, its unmodified analogue ($\Delta T_m = -3$ °C). Other singly modified duplexes show similar behavior. Incorporating two metal-containing nucleosides on the same strand (e.g., **18·20**) results in additional destabilization ($\Delta T_m = -8$ °C). On the other hand, a metal-containing nucleoside at the 5′-end of the duplex **17·20** is slightly stabilizing ($\Delta T_m = +1$ °C), and a duplex containing two modification, one terminal and one internal (**17·19**), is as stable as the parent unmodified duplex (Table 3).[29]

Several factors may influence the relative stability of the modified metal-containing oligonucleotides. These include electrostatic, steric, and solvation effects. While the introduction of a positively charged metal complex is expected to electrostatically stabilize the duplex, the presence of large aromatic ligands in the major groove might cause the opposite effect by repealing water molecules and bound small cations. To a large extent, these opposite effects appear to cancel one another. These considerations are likely to be less important when a metal-containing nucleosides is incorporated at the ends of the double-stranded structures. In this situation, electrostatic stabilization may be the dominating factor, as experimentally observed.

To determine the effect of metal modification on the overall structural integrity of the DNA double helix, the CD spectra of

(29) The destabilization observed for singly modified duplexes is far smaller than the effect of a single mismatch on duplex stability as previously demonstrated (ref 8).

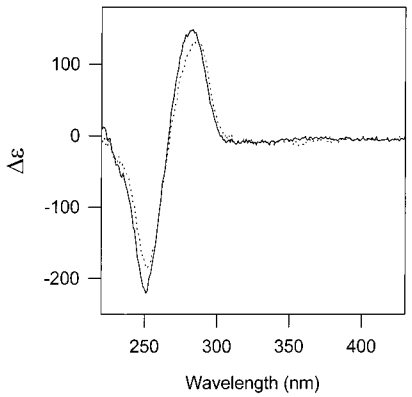

Figure 9. CD spectra of a 2 μM solution of an unmodified 20-mer duplex **14·20** (solid line) and the Ru^{II}-containing 20-mer duplex **15·20** (dotted line) in 10 mM phosphate buffer, pH 7.0, and 100 mM NaCl.

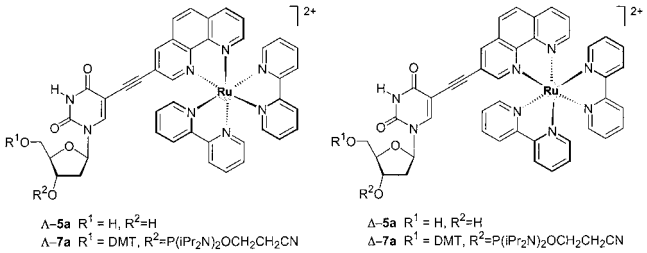

Figure 10. Structures of diastereomerically pure nucleosides Λ-**5a** and Δ-**5a** and their corresponding phosphoramidites Λ-**7a** and Δ-**7a**.

the duplex **15·20** and a control unmodified duplex **14·20** were compared (Figure 9). The spectrum of the metal-containing duplex exhibits a negative band at 252 nm, a crossover at 266 nm, and a positive band at 286 nm. This spectrum is similar to the spectrum obtained for the unmodified duplex. These spectra indicate that metal-modification placed in the major groove does not interfere with the formation of a B-form duplex DNA.[30]

Diastereomerically Pure Nucleosides and Oligonucleotides. When an octahedral metal ion is coordinated to three bidentate ligands, two enantiomeric complexes, Λ and Δ, are formed. To control the absolute configuration at the metal center within the modified DNA duplexes, we have synthesized the diastereomerically pure nucleosides Λ-**5a** and Δ-**5a** and their corresponding phosphoramidites Λ-**7a** and Δ-**7a** (Figure 10). We have followed an identical synthetic scheme where 5-ethynyldeoxyuridine **2** was cross-coupled to the enantiomerically pure Λ-**4a** and Δ-**4a** (Scheme 1).[23,31] The CD spectra of the diastereoisomeric nucleosides Λ-**5a** and Δ-**5a** are shown in Figure 11 and compared to a 1:1 mixture of the two epimers (i.e., **5a**). As expected, the CD spectra are dominated by the coordinated polypyridine chromophores, and the two epimeric nucleosides give rise to essentially mirror-imaged patterns. Typical excitonic interactions of the ligand-centered $\pi-\pi^*$ transitions,[32] and the strong Cotton effects observed for the visible MLCT bands, confirm the assigned absolute configuration at the metal centers.[31,32] Importantly, the diastereomeric metal-containing nucleosides Λ-**5a** and Δ-**5a** emit at the same wavelength (632 nm) upon excitation at their MLCT bands and display identical excited-state lifetimes (1.07 μs).

(30) As expected, no "spectral" interference is observed by the appended polypyridine complexes since a 1:1 mixture of the Δ and Λ metal centers is present. This isolates the effect of the metal complex on the global structure of the modified double helices.
(31) Tzalis, D.; Tor, Y. *J. Am. Chem. Soc.* **1997**, *119*, 852−853.
(32) Bosnich, B. *Acc. Chem. Res.* **1969**, *2*, 266−273.

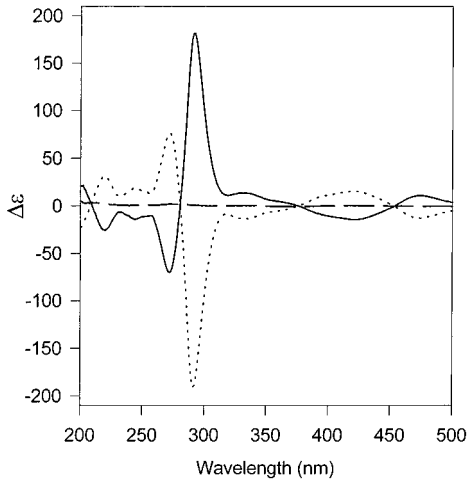

Figure 11. CD spectra of Λ-**5a** (solid line), Δ-**5a** (dotted line), and epimeric **5a** (dashed line) in isoabsorptive acetonitrile solutions.

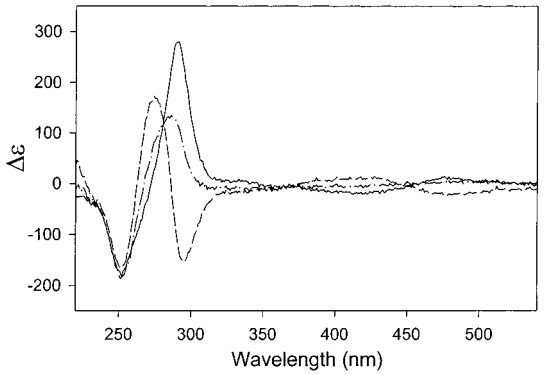

Figure 12. CD spectra of 20-mer DNA duplexes incorporating disatereomerically pure Ru^{II} nucleosides. Shown are duplexes Λ-**15·20** (solid line), Δ-**15·20** (dashed line), and the epimeric **15·20** duplex containing the two enantiomeric metal centers (−·−·) in 10 mM phosphate buffer, pH 7.0, and 100 mM NaCl.

Once incorporated into oligonucleotides, the subtle stereochemical perturbation at the metal center is manifested at different levels. The diastereomeric nature of the two duplexes Λ-**15·20** and Δ-**15·20** is clearly reflected in their CD spectra (Figure 12),[33] where the strong excitonic interaction of the coordinated ligands overlap with those derived from the DNA bases. In the Λ-Ru^{II}-modified duplex, the strong positive transition of the aromatic polypyridine ligands at 290 nm overlaps with the transitions generated by the heterocyclic bases in the same spectral region, resulting in an overall enhancement of the band observed below 300 nm. In contrast, the Δ-Ru^{II} modified 20-mer shows a unique pattern resulting from the opposite excitonic transitions that overlap with the typical B-DNA circular dichroism commonly observed for unmodified duplexes. The mirrored CD effects of the Λ- and Δ-Ru^{II} nucleosides can be distinctly seen in the visible region where the DNA has no absorption. In regions where the circular dichroism signals of the metal complexes are weak (e.g., below 250 nm), the typical CD spectrum of a B-form DNA predominates. This is particularly apparent at a crossover point in the CD spectra of the diastereomerically pure metalated nucleosides (e.g., at 280 nm). At this wavelength, the transitions of the diastereoisomeric duplexes perfectly intersect that of the duplex containing the racemic metal complexes.[34]

(33) The prefix Λ or Δ designates the absolute configuration at the metal center.

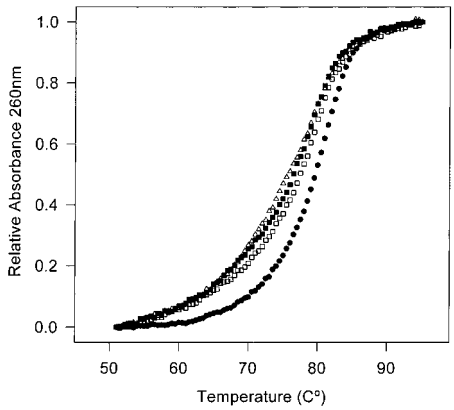

Figure 13. Thermal denaturation curves of diastereomerically pure Ru^{II}-modified DNA 20-mers in 10 mM phosphate buffer pH 7.0, 100 mM NaCl. Shown are **Λ-15·20** (□), **Δ-15·20** (△), "racemic" **15·20** (■), and the unmodified control duplex **14·20** (●).

Although the rigidly linked metal complexes are projected into the major groove of the duplex, the ancillary bipyridine ligands around the metal centers may influence the fit within the groove. To test this plausible effect, the relative stability of the diastereoisomeric duplexes have been examined. The thermal melting curves of the diasteromerically pure Ru^{II} duplexes **Λ-15·20** and **Δ-15·20** are very similar to that obtained for the "racemic" duplex **15·20** (Figure 13). All show a slight destabilization of 2−3 °C when compared to the corresponding unmodified 20-mer duplex **14·20** (T_m = 79 °C). Although nearly identical T_m values for the diastereomerically pure duplexes are obtained, subtle differences in the shape of the curves are likely due to the chiral metal center. As discussed below, a better insight into the differential accommodation of the enantiomeric metal centers in the groove is obtained the investigating the photophysical characteristics of the diastereomeric oligonucleotides.

Photophysical Properties of Metal-Containing Oligonucleotides. The absorption spectra of metalated single-stranded oligonucleotides in degassed 10 mM phosphate buffer pH 7.0, and 100 mM NaCl are dominated by an intense band at 260 nm resulting from the $\pi-\pi^*$ transitions of the heterocyclic DNA bases, with a weak shoulder at 290 nm arising from the ligand-centered transitions of the metal-containing nucleosides (see Figure 8 for an example). Lower energy transitions at around 350 nm are characteristic of the extended conjugation of the pyrimidine-linked phenanthroline ligand. The metalated oligonucleotides also exhibit the characteristic MLCT bands of the corresponding ruthenium or osmium metal complexes (450 and 440−500 nm, respectively).

Table 4 summarizes the steady-state and time-resolved luminescence data for representative oligonucleotides. Excitation of the metal-modified single strands at 450 nm leads to a strong emission centered at 632 nm for the Ru^{II}-oligonucleotides, and a substantially weaker emission at 740 nm for the Os^{II}-containing strands. The emission intensity of the polypyridyl-metal centers in the nucleosides remains relatively unchanged upon incorporation into single stranded oligonucleotides. Time-resolved luminescence spectroscopy shows, however, significant differences between the excited-state behavior of the metal-containing nucleosides and metalated oligonucleotides. The Ru^{II}-nucleosides **5a** and Os^{II}-nucleoside **5b** exhibit a monoexponential luminescence decay in aqueous solutions. In contrast, both the Ru^{II}- and Os^{II}-modified single strands **15** and **16**, respectively, display biexponential emission decays with a slightly longer average luminescence lifetime than the nucleosides.[35] Both single-stranded metal−DNA conjugates exhibit a long-lived component of the excited state that comes closer to the lifetime observed for the corresponding nucleosides in organic acetonitrile solutions. This may suggest a certain degree of protection of the complex-centered excited state from the bulk aqueous solvent by neighboring bases.[36,37]

Table 4. Spectroscopic Data for Metal-Containing Single Strands and Duplexes[a]

samples	$\langle\tau\rangle$ (μs)[b]	τ1 (μs)	A1 (%)	τ1 (μs)	A2(%)	λ_{em}[c]
15	1.17	1.54	55	0.72	45	632
16	0.032	0.08	15	0.024	85	740
17	1.23	1.63	49	0.85	51	627
15·20	1.12	1.91	28	0.83	72	629
Λ-15·20	1.10	2.03	20	0.87	80	633
Δ-15·20	1.13	1.78	40	0.71	60	622
16·20	0.027	0.08	10	0.021	90	740
15·19	0.43	1.02	37	0.08	63	624
Λ-15·19	0.39	1.07	35	0.07	65	629
Δ-15·19	0.42	0.94	37	0.08	63	616

[a] All measurements were performed with 2 μM deoxygenated solutions in 100 mM NaCl, 10 mM phosphate, pH 7.0 at room temperature. Samples **15-17** and **15·20** were excited at 450 nm. Emission decays were monitored at 630 nm for Ru^{II} samples and 740 for Os^{II} samples, and were analyzed according to the biexponential function: $I_{em}(t) = A_1\exp(-t/\tau_1) + A_2\exp(-t/\tau_2)$. Samples **15·19** were excited at the isosbestic point for the absorption of the Ru^{II}- and Os^{II}-modified free nucleosides (467 nm). Emission decays were monitored at 630 nm. [b] Average lifetimes $\langle\tau\rangle$ were calculated from $\langle\tau\rangle = A_1\tau_1 + A_2\tau_2$. [c] Emission maxima were determined by steady-state fluorescence.

In Ru^{II}-containing oligonucleotides, hybridization to a complementary strand results in 8−15% decrease in the steady-state emission intensity when compared to both the Ru^{II}-modified nucleoside or single strand oligonucleotide (Figure 14). This diminished luminescence depends on the sequence and positioning of the emitting nucleotide within the duplex. Time-resolved studies show that the Ru^{II} center within the metalated duplexes is also characterized by a biexponential luminescence decay, accompanied by a slight decrease in the averaged excited-state lifetime (Table 4). Unlike the single strands, the decay of both the Ru^{II} and Os^{II}-containing duplexes are dominated by the short-lived component.[38] Duplex formation also results in the partial protection of the excited state from the bulk solvent. This

(34) The typical excitonic interactions of the polypyridyl $\pi-\pi^*$ transitions and the strong Cotton effects observed for the visible MLCT bands confirm the retention of absolute configuration at the metal centers during automated DNA synthesis.

(35) Altering the position of the metal-complex within the oligonucleotide has little effect on either the averaged excited-state lifetime of the relative distribution of the biexponential components (compare **15** and **17** in Table 4).

(36) The presence of a substantially shorter-lived component in the Ru^{II}-containing oligonucleotides may suggest the involvement of an intrastrand reductive quenching mechanism by guanine bases. The redox potential for G oxidation in DNA has been estimated to be around 1.15 V vs SCE (Johnston, D. H.; Glasgow, K. C.; Thorp, H. H. *J. Am. Chem. Soc.* **1995**, *117*, 8933−8938; see also Leconte, J.-P.; Kirsch-De Mesmaeker, A.; Feeney, M.; Kelly, J. M. *Inorg. Chem.* **1995**, *34*, 6481−6491). On the basis of our measurements, nucleoside **5a** displays an uphill driving force for G oxidation of only 0.1 V, which is significantly lower than might have been anticipated. Preliminary Stern−Volmer titrations of the nucleoside **5a** with GMP have not shown, however, appreciable quenching of the Ru^{II}-based emission.

(37) The short-lived component of the Os^{II}-containing oligo **16** is very close to the lifetime of the free nucleoside **5b**. Since the excited state of the Os^{II} is likely to be less redox active than that of the Ru^{II}, this observation further supports the partial involvement of reductive quenching processes in Ru^{II}-containing single stranded oligonucleotides.

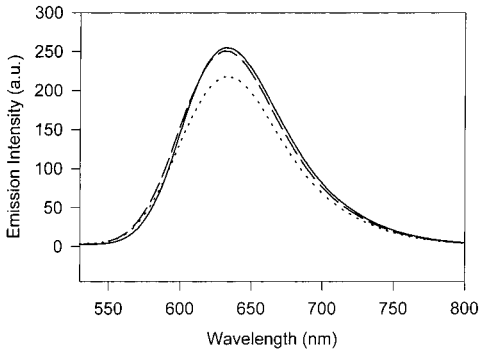

Figure 14. Steady-state emission spectra of isoabsorptive solutions of Ru^{II}-containing nucleoside **5a** (solid line), Ru^{II}-containing single-strand oligonucleotide **15** (dashed line), and the Ru^{II}-containing duplex **15·20** (dotted line) in 10 mM phosphate buffer, pH 7.0, and 100 mM NaCl. Excitation wavelength: 450 nm.

is manifested by the presence of a long-lived component of the excited state. In the Ru-duplex **15·20**, this component of the excited state lifetime is nearly 2-fold longer than that of the Ru^{II} nucleoside **5a** in solution. The Os^{II} duplex **16·20** exhibits the same behavior, with an excited state lifetime component nearly 3-fold longer than the Os^{II} nucleoside **5b** (Table 4).

Through the incorporation of octahedral Ru^{II} centers with predetermined absolute configuration, it is possible to more closely probe the interaction between the metal complexes and the DNA duplex. The photophysical data for the diastereomerically pure duplexes Λ-**15·20** and Δ-**15·20** were compared to those of the epimeric **15·20** duplex (Table 4). When these diastereomeric duplexes were irradiated at 450 nm, steady-state luminescence revealed a 10-nm difference in their emission wavelengths (Table 4 and Figure 15). The Λ-duplex exhibits a strong emission at 633 nm, while the Δ-duplex showed a blue-shifted emission of equal intensity at 622 nm. The emission of the epimeric mixture **15·20** was centered around 629 nm, thus falling between those of the diastereomerically pure duplexes (Figure 15). As discussed above, the metal-based emission of the free Ru^{II} nucleoside is sensitive to solvent polarity. The metal-based emission of the Λ-Ru^{II} center at 633 nm, when attached to the DNA via the ethynyl linker, is indicative of a more polar environment that would stabilize the charge separated excited state. In contrast, the 622 nm emission of the Δ-Ru^{II} center, when incorporated in DNA, suggests a less polar environment for the complex. Importantly, the emission wavelengths of the diastereomerically pure free nucleosides in aqueous solution are identical to that of the "racemic" nucleoside, all emitting at 632 nm (Figure 15).

As seen in the time-resolved luminescence studies of the metal-modified single strands, the duplexes **15·20**, Λ-**15·20**, and Δ-**15·20** also exhibit biexponential decay kinetics (Table 4). Although the average luminescence lifetime found for the Λ- and Δ-Ru^{II} duplexes are nearly equal (1.10 and 1.13 μs, respectively), the relative contributions of the long- and short-lived decay components associated with the diastereomerically pure duplexes are distinctly different. In the Λ-Ru^{II} duplex, the Ru^{II} excited state decays with $\tau 1 = 2.03$ μs (20%) and $\tau 2 = 0.87$ μs (80%). The Δ-Ru^{II} duplex decays with $\tau 1 = 1.78$ μs (40%) and $\tau 2 = 0.71$ μs (60%). In the racemic Ru^{II} duplex, the

(38) This could indicate increased electronic coupling of the metalated base with G residues within the base pair stack, resulting in quenching of the excited state.[36]

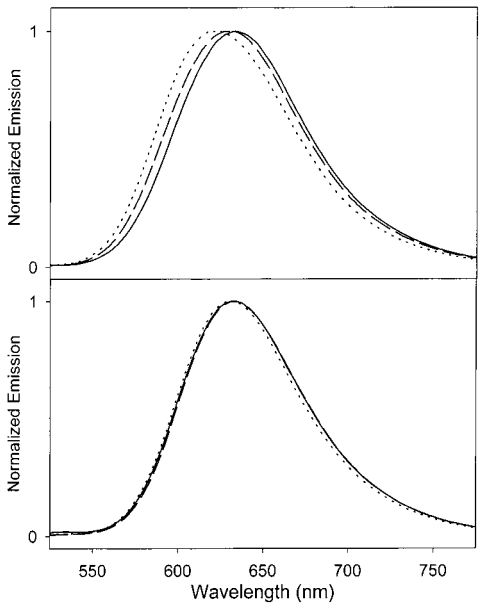

Figure 15. Top: Steady-state emission spectra of isoabsorptive solutions of duplexes Λ-**15·20** (solid line), Δ-**15·20** (dotted line) and epimeric **15·20** (dashed line). Bottom: Steady-state emission spectra of isoabsorptive solutions of nucleosides Λ-**5a** (solid line), Δ-**5a** (dotted line), and epimeric **5a** (dashed line). All spectra were taken in 10 mM phosphate buffer, pH 7.0, and 100 mM NaCl. Excitation wavelength: 450 nm.

distribution of the components of the biexponential decay is nearly the average of the results obtained with the diastereomerically pure duplexes, with $\tau 1 = 1.91$ μs (28%) and $\tau 2 = 0.83$ μs (72%).[39] The larger contribution of the long-lived component in the excited Δ-Ru duplex, together with its shorter emission wavelength, suggest that the Δ-Ru complex fits more tightly into the major groove than does the Λ-Ru complex.[40,41]

Summary

A novel and powerful approach for the site-specific incorporation of polypyridylmetal complexes into synthetic oligonucleotides using automated phosphoramidite chemistry has been established. The methodology is based on metal-containing nucleosides, where the complexes $[(bpy)_2M(3\text{-ethynyl-}1,10\text{-phenanthroline})]^{2+}$ (M = Ru, Os) are covalently attached to the 5-position in 2′-deoxyuridine. These Ru^{II} and Os^{II} building

(39) It is important to note that in all duplexes discussed, the absorption bands at 350 nm are equally suppressed when compared to the nucleoside **5a** in solution. This suggests that the differences in the excited-state lifetimes in the diastereomerically pure oligonucleotides are not due to differential shielding of the excited complex from solvent, but rather can be attributed to a different rotamer population around the ethynyl linkage enforced by the groove walls.

(40) The observation that the Δ isomer is better protected from solvent agrees with Barton's early observations with noncovalently bound $Ru(phen)_3^{2+}$. See Barton, J. K.; Danishefsky, A. T.; Goldberg, J. M. *J. Am. Chem. Soc.* **1984**, *106*, 2172−2176.

(41) To evaluate the influence of the absolute configuration at the Ru^{II}-donor metal center on quenching efficiency, the bis-hetero-metalated duplex **15·19** has been investigated (Table 4). Duplex **15·20** with the appropriate stereochemistry at the donor center has served as a reference. The Ru^{II} emission in duplex Δ-**15·19** suffers 80% quenching while the fraction quenched in the Λ-**15·19** duplex amounts to only 72%. The duplex incorporating a racemic Ru^{II} center exhibits 75% quenching (fraction quenched $= 1 - I_{Ru-Os}/I_{Ru}$ where I represents the integrated emission curve; error is ± 3%). In agreement with the lifetime measurements discussed above, the Δ complex appears to be better accommodated within the chiral major groove. These observations indicate that quenching by the racemic Os^{II} center is dependent, albeit to a small extent, on the absolute configuration at the Ru^{II}-donor metal center. The relatively small magnitude of the effect suggests, therefore, that metal-containing oligonucleotides with racemic metal centers can be utilized for most investigations of donor−acceptor interactions in such assemblies.

blocks are converted into their phosphoramidites and are utilized for the efficient synthesis of modified oligonucleotides.

The metal-containing oligonucleotides form stable duplexes that retain the B-form conformation. The relative stability of the modified duplexes is dependent on the number and position of the metal centers as well as on the sequence composition of the oligonucleotides. The absolute configuration of these rigidly linked metal complexes has little effect on the thermal stability of the oligonucleotides, although photophysical studies suggest the Δ complex is slightly better accommodated within the major groove.

The Ru^{II} center in the nucleoside, oligonucleotides, and double-stranded DNA sequences is luminescent. Absorption and emission spectroscopies demonstrate that the emissive charge separated MLCT excited state is susceptible to environment polarity and suggest that the promoted electron is localized on the extended heterocycle-linked phenanthroline. Delocalization of this excited-state electron density through the conjugated acetylene linker and onto the base-stacked heterocycle is a key feature for exploring energy and electron-transfer processes through the DNA base stack.[42]

Experimental Section

General. NMR spectra were obtained on a Varian Mercury 400 MHz spectrometer. The ^{1}H chemical shifts of nonexchangeable protons are expressed relative to the residual solvent signal of acetonitrile at δ 1.94. The ^{13}C chemical shifts are referenced relative to CD_3CN at δ 1.30. The ^{31}P chemical shifts for metal containing species were measured using the PF_6^- counterion as an internal standard. Infrared spectra were obtained on a Perkin-Elmer 1600 FT-IR spectrometer. Absorption spectra were recorded using an Hewlett-Packard 8452A diode array spectrophotometer. Emission spectra were collected on a Perkin-Elmer LS 50B luminescence spectrophotometer. Optical rotations were determined at ambient temperature using a Perkin-Elmer 241 polarimeter. Electrochemical measurements were performed with a BAS CV-50W system using platinum working and auxiliary electrodes with an $Ag/AgNO_3/CH_3CN$ reference electrode at a 100 mV/s scan rate. The experiments were conducted using 1 mM degassed acetonitrile solutions with 0.1 M [n-Bu_4N^+][PF_6^-] as the supporting electrolyte unless otherwise stated. Ferrocene was used as an external reference. Mass spectral analyses were performed by the University of California-Riverside Mass Spectrometry Facility, and the mass value for the most intense signal of an isotopomeric cluster is reported (see Supporting Information of ref 8 for representative experimental and simulated spectra). HPLC analyses were performed on a Hewlett-Packard 1050 series analytical HPLC using a Vydac reversed-phase column (0.46 × 25 cm, 5μ C18-silica). HPLC grade solvents were obtained from Fisher Scientific. Flash chromatography was performed using silica gel 60 (230−400 mesh, Merck) or activated basic aluminum oxide (50−200 micron, Acros). Thin-layer chromatography (TLC) was performed using silica gel 60 F_{254} precoated plates (Merck). Visualization was done by UV (254 nm) and by treatment with a solution of 4 g of cerium (IV) sulfate, 100 g of ammonium molybdate, 100 mL of sulfuric acid, and 900 mL of water, followed by heating. 4,4′-Dimethoxytrityl chloride and 2-cyanoethyl-*N*,*N*,*N*′,*N*′-tetraisopropylphosphordiamidite were obtained from Aldrich. All reaction flasks used for DMT-derivatized compounds were treated with a concentrated NaOH prior to use. Nucleoside phosphoramidite monomers as well as ancillary reagents for nucleic acid synthesis were obtained from Prime Synthesis, Inc. (Aston, PA). Anhydrous acetonitrile, pyridine, dichloromethane, and *N*,*N*′-dimethylformamide, stored over 4-Å molecular sieves, were obtained from Fluka. Unless otherwise specified, materials obtained from commercial suppliers were used without further purification.

Compound 3. Nucleoside **2**[14,15] (500 mg, 1.98 mmol), 4,4′-dimethoxytrityl chloride (772 mg, 2.28 mmol), and 4-(dimethylamino)-pyridine (22 mg, 0.20 mmol) were suspended in anhydrous pyridine (7 mL) and triethylamine (250 μL). The solution was stirred for 2 h at room temperature under argon, then evaporated under reduced pressure to an amber foam. The crude product was purified by flash chromatography on silica gel. The column was eluted first with 0.5% triethylamine, 1% methanol in dichloromethane to remove impurities, followed by stepwise increase to 4% methanol. The product was obtained as a light yellow foam in 92% yield (987 mg). TLC (7% $MeOH/CH_2Cl_2$) $R_f = 0.26$; IR (KBr): 2115 cm^{-1} (−C≡CH); ^{1}H NMR (CD_3CN, 400 MHz): δ 7.95 (s, 1H), 7.45 (d, J = 7.7 Hz, 2H), 7.35 (d, J = 8.8 Hz, 4H), 7.31 (t, J = 8.1 Hz, 2H), 7.23 (t, J = 7.3 Hz, 1H), 6.88 (dd, J = 8.8, 2.6 Hz, 4H), 6.13 (t, J = 6.6 Hz, 1H, H-1′), 4.42−4.46 (m, 1H, H-3′), 3.96−3.98 (m, 1H, H-4′), 3.77 (s, 6H, $-OCH_3$), 3.32 (dd, J = 11.0, 4.8 Hz, 1H, H-5′$_A$), 3.21 (dd, J = 10.6, 2.6 Hz, 1H, H-5′$_B$), 3.16 (s, 1H, −C≡C*H*), 2.23−2.32 (m, 2H, H-2′); ^{13}C NMR (CD_3CN, 101 MHz): δ 41.53, 55.96, 64.46, 72.01, 76.27, 82.66, 86.63, 87.41, 87.59, 99.23, 114.27, 114.29, 128.01, 129.09, 131.15, 131.21, 136.80, 137.05, 145.33, 146.13, 150.56, 159.89, 162.82; ESI MS calcd for $C_{32}H_{30}N_2O_7Na$ 577.580 $[MNa]^+$, found 577.

Compound 5a. Ru^{II} complex **4a**[13] (150 mg, 0.16 mmol), (dppf)-$PdCl_2$·CH_2Cl_2 (6 mg, 0.008 mmol), and CuI (1.5 mg, 0.008 mmol) were dissolved in a degassed solution of anhydrous DMF (1.5 mL) and triethylamine (150 μL) under argon. A solution of nucleoside **2** (43 mg, 0.17 mmol) in a degassed solution of anhydrous DMF (1.5 mL) and triethylamine (150 μL) was added over 5 min. The solution was stirred under argon for 3 h at room temperature, and then evaporated under reduced pressure. The crude reaction mixture was purified by flash chromatography (silica gel, 1% saturated aqueous KPF_6, 6% water in acetonitrile). The product fractions were concentrated, dissolved in cold 1:3 acetone/dichloromethane, and filtered to remove excess KPF_6. The product solution was dried, suspended in water, and filtered. The product **5a** was obtained as a mixture of diastereomers in 81% yield (143 mg) as red solid. TLC (1% saturated aqueous KNO_3/10% H_2O/CH_3CN) $R_f = 0.13$; $[\alpha]_D^{21} = -38$, (c = 0.1 mg/mL in CH_3CN); IR (KBr): 2216 cm^{-1} (-C≡C-); ^{1}H NMR (CD_3-CN, 400 MHz): δ 9.34 (s, 1H), 8.65 (d, J = 1.5 Hz, 1H), 8.62 (dd, J = 8.3, 1.0 Hz, 1H), 8.52−8.57 (m, 3H), 8.50 (d, J = 8.3 Hz, 1H), 8.34 (s, 1H), 8.27 (d, J = 8.8 Hz, 1H), 8.20 (d, J = 8.8 Hz, 1H), 8.08−8.13 (m, 4H), 8.02 (dt, J = 8.1, 1.5 Hz, 1H), 8.01 (dt, J = 8.1, 1.5 Hz, 1H), 7.87 (d, J = 4.9 Hz, 1H), 7.81 (d, J = 4.9 Hz, 1H), 7.75 (dd, J = 8.3, 5.4 Hz, 1H), 7.65 (d, J = 5.9 Hz, 1H), 7.53 (d, J = 4.9 Hz, 1H), 7.44−7.48 (m, 2H), 7.24−7.26 (m, 2H), 6.11 (dt, J = 6.6, 1.6 Hz, 1H, H-1′), 4.33−4.36 (m, 1H, H-3′), 3.90−3.92 (m, 1H, H-4′), 3.70−3.78 (m, 2H, H-5′), 2.26−2.31 (m, 1H, H-2′$_A$), 2.14−2.20 (m, 1H, H-2′$_B$); ^{13}C NMR (CD_3CN, 101 MHz): δ 41.52, 61.89, 61.91, 70.98, 71.00, 86.77, 86.81, 88.09, 88.11, 88.51, 88.53, 89.32, 98.02, 98.04, 122.85, 124.95, 125.04, 125.10, 125.12, 127.05, 128.17, 128.24, 128.37, 128.39, 128.47, 129.71, 131.10, 132.14, 137.67, 138.57, 138.59, 138.72, 138.73, 139.06, 139.09, 146.31, 147.01, 148.06, 150.01, 152.66, 152.70, 152.89, 152.93, 153.00, 153.60, 154.28, 157.63, 157.76, 157.99, 158.02, 161.76; UV (CH_3CN): λ_{max} nm ($\epsilon \times 10^{-3}$) 242 (39.7), 256 (39.0), 286 (69.3), 352 (27.1), 450 (12.6); ϵ_{260} = 36,500; ESI MS calcd for $C_{43}H_{34}F_6N_8O_5PRu$ $[M]^+$ 988.815, found 989 $[M]^+$, 422 $[M]^{2+}$.

Compound Λ-5a. The nucleoside **Λ-5a** was obtained by the same procedure described above for **5a** from nucleoside **2** and **Λ-4a** (see ref 31 for the resolution procedure). The product was obtained in a 71% yield as a red foam. TLC (1% saturated aqueous KNO_3/10% H_2O/CH_3CN) $R_f = 0.13$; $[\alpha]_D^{21} = +451$, (c = 0.1 mg/mL in CH_3CN); CD (CH_3CN) 210 (0), 220 (−25.1), 244 (−14.2), 272 (−69.9), 281 (0), 292 (181.8), 332 (13.6), 377 (0), 424 (−14.2), 454 (0), 475 (11.2); ^{1}H NMR (CD_3CN, 400 MHz): δ 8.65 (d, J = 1.5 Hz, 1H), 8.60 (dd, J =

(42) The effect of donor/acceptor separation, relative placement, sequence, and degree of electronic conjugation on photophysical processes in metalated DNAs is systematically investigated in our laboratories. These results will be communicated in due course.

8.1, 1.1 Hz, 1H), 8.47−8.55 (m, 4H), 8.40 (s, 1H), 8.25 (d, J = 8.8 Hz, 1H), 8.19 (d, J = 8.8 Hz, 1H), 8.06−8.12 (m, 4H), 8.00 (dt, J = 7.7, 1.5 Hz, 1H), 7.99 (dt, J = 7.1, 1.5 Hz, 1H), 7.86 (d, J = 5.1 Hz, 1H), 7.79 (d, J = 4.4 Hz, 1H), 7.73 (dd, J = 8.1, 5.1 Hz, 1H), 7.64 (d, J = 4.4 Hz, 1H), 7.50 (d, J = 4.8 Hz, 1H), 7.46 (dt, J = 6.8, 1.1 Hz, 1H), 7.44 (dt, J = 6.0, 1.1 Hz, 1H), 7.23 (t, J = 6.6 Hz, 2H), 6.07 (t, J = 5.9 Hz, 1H, H-1′), 4.32−4.36 (m, 1H, H-3′), 3.86−3.87 (m, 1H, H-4′), 3.71−3.78 (m, 2H, H-5′), 2.26−2.32 (m, 1H, H-2′$_A$), 2.14−2.19 (m, 1H, H-2′$_B$); ^{13}C NMR (CD_3CN, 101 MHz): δ 41.51, 61.69, 70.61, 86.75, 88.15, 88.63, 89.53, 98.03, 122.99, 125.05, 125.14, 125.22, 125.25, 127.14, 128.29, 128.33, 128.49, 128.51, 128.60, 129.80, 131.22, 132.24, 137.79, 138.67, 138.71, 138.83, 138.86, 139.19, 146.52, 147.10, 148.19, 150.14, 152.80, 152.81, 153.04, 153.16, 153.71, 154.42, 157.76, 157.91, 158.15, 161.88; ESI MS calcd for $C_{43}H_{34}F_6N_8O_5PRu$ $[M]^+$ 988.815, found 989 $[M]^+$, 422 $[M]^{2+}$.

Compound Δ-5a. The nucleoside Δ-**5a** was obtained by the same procedure described above for **5a** from nucleoside **2** and Δ-**4a** (see ref 31 for the resolution procedure). The product was obtained in a 64% yield as a red foam. TLC (1% saturated aqueous KNO_3/10% H_2O/CH_3CN) R_f = 0.13; $[\alpha]_D^{21}$ = −594, (c = 0.1 mg/mL in CH_3CN); CD (CH_3CN) 209(0), 219 (31.4), 244 (18.7), 272 (76.7), 281 (0), 291 (−190.8), 332 (−13.7), 376 (0), 421 (15.7), 453 (0), 475 (12.6); ^{1}H NMR (CD_3CN, 400 MHz): δ 9.34 (s, 1H), 8.65 (d, J = 1.5 Hz, 1H), 8.61 (dd, J = 8.2, 1.1 Hz, 1H), 8.48−8.56 (m, 4H), 8.35 (s, 1H), 8.26 (d, J = 8.8 Hz, 1H), 8.20 (d, J = 8.8 Hz, 1H), 8.07−8.13 (m, 4H), 8.02 (dt, J = 7.7, 1.5 Hz, 1H), 8.00 (dt, J = 7.9, 1.5 Hz, 1H), 7.86 (d, J = 4.8 Hz, 1H), 7.79 (d, J = 5.1 Hz, 1H), 7.74 (dd, J = 8.4, 5.5 Hz, 1H), 7.64 (d, J = 5.1 Hz, 1H), 7.52 (d, J = 5.1 Hz, 1H), 7.46 (dt, J = 6.2, 1.5 Hz, 1H), 7.45 (dt, J = 6.0, 1.1 Hz, 1H), 7.24 (t, J = 6.2 Hz, 2H), 6.10 (t, J = 6.2 Hz, 1H, H-1′), 4.32−4.36 (m, 1H, H-3′), 3.89−3.91 (m, 1H, H-4′), 3.69−3.78 (m, 2H, H-5′), 2.26−2.32 (m, 1H, H-2′$_A$), 2.14−2.19 (m, 1H, H-2′$_B$); ^{13}C NMR (CD_3CN, 101 MHz): δ 41.56, 61.97, 71.07, 86.91, 88.21, 88.65, 89.40, 98.16, 122.99, 125.11, 125.20, 125.25, 125.28, 127.21, 128.33, 128.41, 128.52, 128.55, 128.63, 129.87, 131.26, 132.31, 137.84, 138.74, 138.76, 138.89, 138.90, 139.27, 146.51, 147.20, 148.24, 150.20, 152.84, 152.89, 153.12, 153.18, 153.79, 154.47, 157.82, 157.94, 158.18, 158.20, 162.00; ESI MS calcd for $C_{43}H_{34}F_6N_8O_5PRu$ $[M]^+$ 988.815, found 989 $[M]^+$, 422 $[M]^{2+}$.

Compound 5b. A mixture of nucleoside **2** (16 mg, 0.062 mmol), Os^{II} complex **4b** (50 mg, 0.048 mmol), Pd(dppf)Cl_2·CH_2Cl_2 (3 mg, 0.004 mmol), and CuI (0.5 mg, 0.003 mmol) was dissolved in a degassed solution of anhydrous DMF (1.5 mL) and triethylamine (100 μL) under argon. The solution was sonicated for 8 h at 50 °C, then the solvent removed under reduced pressure. The crude reaction mixture was purified by flash chromatography (silica gel, 1% saturated aqueous KPF_6, 8% water in acetonitrile). The product fractions were concentrated, dissolved in cold 1:3 acetone/dichloromethane, and filtered to remove excess KPF_6. The product solution was dried, suspended in water, and filtered. The product **5b** was obtained as a mixture of diastereomers in 86% yield (50 mg) as a dark brown foam. TLC (1% saturated aqueous KNO_3/10% H_2O/CH_3CN) R_f = 0.13; IR (KBr): 2216 cm^{-1} (-C≡C-); ^{1}H NMR (CD_3CN, 400 MHz): δ 9.31 (s, 1H), 8.49−8.54 (m, 3H), 8.47 (d, J = 8.3 Hz, 1H), 8.42 (d, J = 1.5 Hz, 1H), 8.40 (d, J = 8.3 Hz, 1H), 8.35 (s, 1H), 8.26 (d, J = 8.8 Hz, 1H), 8.19 (d, J = 8.8 Hz, 1H), 8.03 (s, 1H), 8.00 (d, J = 4.9 Hz, 1H), 7.90−7.93 (m, 2H), 7.80−7.85 (m, 2H), 7.78 (d, J = 5.9 Hz, 1H), 7.71 (d, J = 5.4 Hz, 1H), 7.67 (dd, J = 8.3, 5.4 Hz, 1H), 7.53 (d, J = 5.9 Hz, 1H), 7.41 (d, J = 5.4 Hz, 1H), 7.35−7.39 (m, 2H), 7.13−7.17 (m, 2H), 6.11 (t, J = 6.3 Hz, 1H, H-1′), 4.32−4.35 (m, 1H, H-3′), 3.89−3.91 (m, 1H, H-4′), 3.70−3.77 (m, 2H, H-5′), 2.26−2.30 (m, 1H, H-2′$_A$), 2.15−2.20 (m, 1H, H-2′$_B$); ^{13}C NMR (CD_3CN, 101 MHz): δ 41.54, 61.90, 70.95, 86.82, 86.85, 88.02, 88.04, 88.59, 88.61, 89.49, 98.08, 123.19, 125.24, 125.29, 125.38, 125.40, 127.26, 128.71, 128.76, 128.82, 128.91, 129.88, 131.42, 132.54, 137.45, 138.04, 138.10, 138.22, 138.93, 146.45, 149.59, 150.11, 150.38, 151.84, 152.04, 152.13, 152.17, 152.31, 153.08, 153.86, 159.63, 159.79, 159.96, 159.98, 161.97; UV (CH_3-CN): λ_{max} nm ($\epsilon \times 10^{-3}$) 242 (37.9), 254 (35.6), 290 (64.3), 358 (25.9), 436 (11.1), 484 (11.0), 592 (3.1); ϵ_{260} = 33 200; ESI MS calcd for $C_{43}H_{34}F_6N_8O_5OsP$ $[M]^+$ 1077.975, found 1078 $[M]^+$, 466 $[M]^{2+}$.

Compound 6a. A mixture of nucleoside **3** (484 mg, 0.87 mmol), **4a** (800 mg, 0.83 mmol), Pd(PPh_3)$_2Cl_2$ (29 mg, 0.042 mmol), and CuI (8 mg, 0.042 mmol) was dissolved in a degassed solution of anhydrous DMF (15 mL) and triethylamine (2 mL) under argon. The mixture was sonicated for 8 h at 50 °C under an argon atmosphere and the solvent was removed under reduced pressure. The crude reaction mixture was purified by flash chromatography (basic alumina, 0.5% saturated aqueous KPF_6, 2.5% water in acetonitrile). The product fractions were concentrated, dissolved in dichloromethane, and filtered to remove excess KPF_6. The product **6a** was obtained as a mixture of diastereomers in 83% yield (600 mg) as a red foam. TLC (1% saturated aqueous KNO_3/10% H_2O/CH_3CN) R_f = 0.28; IR (KBr): 2207 cm^{-1} (-C≡C-); ^{1}H NMR (CD_3CN, 400 MHz): δ 8.61 (dd, J = 2.9, 1.2 Hz, 0.5H), 8.59 (dd, J = 2.9, 1.2 Hz, 0.5H), 8.45−8.52 (m, 3H), 8.39 (t, J = 7.1 Hz, 1H), 8.38 (s, 0.5H), 8.27 (s, 0.5H), 8.23 (d, J = 8.8 Hz, 0.5H), 8.21 (d, J = 8.8 Hz, 0.5H), 7.93−8.11 (m, 6.5H), 7.84 (d, J = 5.6 Hz, 0.5H), 7.83 (d, J = 8.8 Hz, 0.5H), 7.77 (d, J = 5.6 Hz, 0.5H), 7.68−7.75 (m, 2H), 7.55 (d, J = 5.6 Hz, 0.5H), 7.49−7.53 (m, 1.5H), 7.35−7.45 (m, 5.5H), 7.30−7.34 (m, 2H), 7.22−7.27 (m, 2.5H), 7.18 (t, J = 5.9 Hz, 0.5H), 7.09 (app quin, J = 7.4 Hz, 2H), 6.97 (t, J = 7.4, 0.5 Hz), 6.84 (t, J = 7.4 Hz, 0.5H), 6.78 (d, J = 9.3 Hz, 1H), 6.74 (d, J = 9.3 Hz, 1H), 6.71 (d, J = 8.8 Hz, 1H), 6.57 (d, J = 9.3 Hz, 1H), 6.14 (dt, J = 6.3, 1.0 Hz, 1H, H-1′), 4.58 and 4.49 (quin, J = 3.9 Hz, 1H, H-3′), 4.01−4.04 and 3.95−3.97 (m, 1H, H-4′), 3.58, 3.57, 3.56, and 3.47 (s, 6H, −OCH_3), 3.40 and 3.37 (d, J = 4.2 Hz, 1H, 3′-OH), 3.34 and 3.14 (dd, J = 10.8, 2.0 Hz, 1H, H-5′$_A$), 3.31 and 3.21 (dd, J = 10.8, 2.0 Hz, 1H, H-5′$_B$), 2.30−2.40 (m, 4H, H-2′); ^{13}C NMR (CD_3-CN, 101 MHz): δ 42.05, 42.08, 55.62, 55.71, 55.76, 63.49, 63.71, 71.36, 71.41, 86.56, 87.14, 87.34, 87.40, 87.44, 87.49, 88.11, 88.20, 89.00, 89.23, 98.20, 98.32, 113.95, 113.98, 114.02, 114.08, 122.53, 122.61, 124.79, 124.95, 125.00, 125.03, 125.08, 127.01, 127.48, 127.76, 128.12, 128.17, 128.22, 128.26, 128.28, 128.30, 128.39, 128.45, 128.61, 18.69, 128.76, 129.53, 129.58, 130.39, 130.54, 130.71, 130.75, 130.81, 132.11, 132.18, 136.23, 136.38, 136.57, 136.80, 137.63, 137.67, 138.58, 138.62, 138.64, 138.69, 139.62, 140.00, 145.27, 145.40, 145.61, 146.03, 146.74, 146.80, 147.93, 149.95, 152.48, 152.56, 152.61, 152.71, 152.76, 152.79, 152.82, 153.54, 153.70, 157.55, 157.58, 157.67, 157.70, 157.83, 157.88, 159.12, 159.29, 159.32, 159.35, 161.91, 161.94; ESI MS calcd for $C_{64}H_{52}F_6N_8O_7PRu$ $[M]^+$ 1291.182, found 1291 $[M]^+$, 573 $[M]^{2+}$.

Compound Λ-6a. Product Λ-**6a** was obtained by the same procedure described above for **6a** from compounds **3** and Λ-**4a** (see ref 31 for the resolution procedure). The product was obtained as a red foam in 74% yield. TLC (1% saturated aqueous KNO_3/10% H_2O/CH_3CN) R_f = 0.28; ^{1}H NMR (CD_3CN, 400 MHz): δ 8.61 (dd, J = 7.8, 1.0 Hz, 1H), 8.53 (d, J = 8.3 Hz, 1H), 8.47−8.50 (m, 3H), 8.40 (s, 1H), 8.23 (d, J = 8.8 Hz, 1H), 8.10 (dt, J = 7.8, 1.0 Hz, 1H), 7.99−8.07 (m, 4H), 7.97 (d, J = 1.5 Hz, 1H), 7.85−7.86 (m, 2H), 7.77 (d, J = 4.9 Hz, 1H), 7.74 (dd, J = 7.8, 4.9 Hz, 1H), 7.52 (t, J = 4.4 Hz, 2H), 7.42−7.46 (m, 5H), 7.39 (d, J = 9.3 Hz, 2H), 7.33 (d, J = 8.8 Hz, 2H), 7.26 (dt, J = 5.4, 1.0 Hz, 1H), 7.19 (dt, J = 5.8, 1.5 Hz, 1H), 7.08 (t, J = 7.3 Hz, 2H), 6.84 (t, J = 7.3 Hz, 1H), 6.79 (d, J = 8.8 Hz, 2H), 6.74 (d, J = 8.8 Hz, 2H), 6.14 (t, J = 6.4 Hz, 1H, H-1′), 4.50−4.52 (m, 1H, H-3′), 4.02−4.04 (m, 1H, H-4′), 3.59 and 3.57 (s, 6H, −OCH_3), 3.40 (d, J = 4.4 Hz, 1H, 3′-OH), 3.34 (dd, J = 10.8, 2.4 Hz, 1H, H-5′$_A$), 3.15 (dd, J = 10.8, 3.4 Hz, 1H, H-5′$_B$), 2.37−2.42 (m, 1H, H-2′$_A$), 2.32−2.36 (m, 1H, H-2′$_B$); ^{13}C NMR (CD_3CN, 101 MHz): δ 42.08, 55.71, 55.76, 63.70, 71.42, 87.13, 87.38, 87.50, 88.07, 89.21, 98.19, 113.97, 114.07, 122.52, 124.95, 124.99, 125.02, 125.07, 126.99, 127.47, 128.11, 128.25, 128.29, 128.38, 128.68, 129.51, 130.54, 130.70, 130.81, 132.10, 136.21, 136.56, 137.62, 138.55, 138.60, 138.67, 138.70, 139.64, 145.59, 146.02, 146.73, 147.92, 149.84, 152.55, 152.61, 152.71,

152.82, 153.52, 157.57, 157.70, 157.82, 157.88, 159.33, 161.71; ESI MS calcd for $C_{64}H_{52}F_6N_8O_7PRu$ $[M]^+$ 1291.182, found 1291 $[M]^+$, 573 $[M]^{2+}$.

Compound Δ-6a. Product Δ-**6a** was obtained by the same procedure described above for **6a** from compounds **3** and Δ-**4a** (see ref 31 for the resolution procedure). The product was obtained as a red foam in 68% yield. TLC (1% saturated aqueous KNO_3/10% H_2O/CH_3CN) R_f = 0.28; ^{1}H NMR (CD_3CN, 400 MHz) δ 8.62 (d, J = 8.3 Hz, 1H), 8.51 (d, J = 8.3 Hz, 1H), 8.49 (d, J = 7.8 Hz, 1H), 8.40 (t, J = 8.3 Hz, 2H), 8.29 (d, J = 1.5 Hz, 1H), 8.25 (dd, J = 8.9, 1.5 Hz, 1H), 8.10 (t, J = 7.8 Hz, 1H), 8.05 (d, J = 5.4 Hz, 1H), 7.97−8.03 (m, 4H), 7.96 (d, J = 8.8 Hz, 1H), 7.80 (d, J = 5.4 Hz, 1H), 7.72−7.75 (m, 3H), 7.58 (d, J = 5.8 Hz, 1H), 7.55 (d, J = 5.4 Hz, 1H), 7.41−7.45 (m, 3H), 7.37 (t, J = 7.8, 1H), 7.34 (dd, J = 8.8, 1.5 Hz, 2H), 7.24−7.28 (m, 4H), 7.12 (t, J = 7.3 Hz, 2H), 6.98 (dt, J = 7.3, 1.0 Hz, 1H), 6.72 (dd, J = 8.8, 1.0 Hz, 2H), 6.57 (dd, J = 8.8,1.0 Hz, 2H), 6.15 (t, J = 6.3 Hz, 1H, H-1′), 4.59−4.61 (m, 1H, H-3′), 3.96−3.98 (m, 1H, H-4′), 3.57 and 3.48 (s, 6H, -OCH_3), 3.32 (dd, J = 10.7, 2.0 Hz, 1H, H-5′$_A$), 3.22 (dd, J = 10.7, 2.0 Hz, 1H, H-5′$_B$), 2.36−2.39 (t, J = 4.9 Hz, 2H, H-2′); ^{13}C NMR (CD_3CN, 101 MHz) δ 42.09, 55.67, 55.75, 63.52, 71.43, 86.61, 87.40, 87.51, 88.24, 89.03, 98.40, 114.03, 114.11, 122.69, 124.88, 125.04, 125.08, 127.11, 127.84, 128.25, 128.31, 128.38, 128.50, 128.54, 128.70, 128.85, 129.67, 129.90, 130.48, 130.80, 130.84, 132.29, 136.47, 136.89, 137.77, 138.68, 138.74, 138.79, 138.83, 140.12, 145.36, 145.49, 146.37, 146.91, 148.02, 149.97, 152.59, 152.88, 152.91, 152.95, 153.66, 153.79, 157.66, 157.69, 157.81, 157.99, 159.25, 159.42, 161.90; ESI MS calcd for $C_{64}H_{52}F_6N_8O_7PRu$ $[M]^+$ 1291.182, found 1291 $[M]^+$, 573 $[M]^{2+}$.

Compound 6b. The dark brown **6b** was obtained by the same procedure described above for **6a** from compounds **3** and Os^{II} complex **4b** as a mixture of diastereomers in 83% yield. TLC (1% saturated aqueous KNO_3/10% H_2O/CH_3CN) R_f = 0.29; IR (KBr): 2207 cm^{-1} (-C≡C-); ^{1}H NMR (CD_3CN, 400 MHz): δ 9.28 (s, 1H), 8.50 (t, J = 7.3 Hz, 1H), 8.44−8.47 (m, 1.5H), 8.36−8.41(m, 2H), 8.38 (s, 0.5H), 8.27 (s, 0.5H), 8.23 (d, J = 9.3 Hz, 0.5H), 8.21 (d, J = 8.8 Hz, 1H), 7.97 (dt, J = 5.4, 1.0 Hz, 1H), 7.94 (d, J = 8.8 Hz, 0.5H), 7.88−7.92 (m, 2H), 7.80−7.86 (m, 3.5H), 7.76 (d, J = 5.4 Hz, 0.5H), 7.70 (d, J = 5.4 Hz, 0.5H), 7.65−7.67 (m, 1.5H), 7.61 (d, J = 5.4 Hz, 0.5H), 7.48 (d, J = 1.5 Hz, 0.5H), 7.29−7.45 (m, 9H), 7.25−7.28 (m, 1.5H), 7.21 (d, J = 1.5 Hz, 0.5H), 7.06−7.17 (m, 4H), 6.98 (t, J = 7.3 Hz, 0.5H), 6.85 (t, J = 7.3 Hz, 1H), 6.79 (d, J = 8.8 Hz, 1H), 6.74 (d, J = 9.3 Hz, 1H), 6.71 (d, J = 8.8 Hz, 1H), 6.57 (d, J = 9.3 Hz, 1H), 6.14 (dt, J = 6.4, 2.0 Hz, 1H, H-1′), 4.57−4.61 and 4.48−5.52 (quin, J = 3.9 Hz, 1H, H-3′), 4.02−4.04 and 3.95−3.97 (m, 1H, H-4′), 3.59, 3.58, 3.57, and 3.48 (s, 6H, -OCH_3), 3.43 and 3.49 (d, J = 4.2 Hz, 1H, 3′-OH), 3.33 and 3.14 (dd, J = 11.2, 3.0 Hz, 1H, H-5′$_A$), 3.31 and 3.20 (dd, J = 10.7, 2.5 Hz, 1H, H-5′$_B$), 2.30−2.40 (m, 2H, H-2′); ^{13}C NMR (CD_3CN, 101 MHz): δ 42.07, 42.10, 55.67, 55.74, 55.79, 63.49, 63.71, 71.39, 71.44, 86.57, 87.16, 87.35, 87.39, 87.46, 87.52, 87.95, 88.03, 89.06, 89.32, 98.20, 98.32, 113.97, 114.00, 114.04, 114.09, 122.78, 122.83, 124.99, 125.13, 125.18, 125.29, 127.17, 127.51, 127.79, 128.40, 128.60, 128.63, 128.71, 128.77, 128.84, 129.64, 129.70, 129.80, 130.41, 130.72, 130.77, 130.84, 130.93, 132.47, 132.55, 136.24, 136.40, 136.59, 136.80, 137.35, 137.34, 137.97, 138.02, 138.09, 138.17, 138.21, 139.50, 139.88, 145.27, 145.42, 145.63, 146.03, 149.26, 149.34, 149.90, 150.14, 150.16, 151.60, 151.68, 151.86, 151.97, 151.99, 152.08, 152.99, 153.01, 153.08, 153.24, 159.16, 159.33, 159.37, 159.45, 159.50, 159.62, 159.67, 159.74, 159.77, 161.82, 161.85; ESI MS calcd for $C_{64}H_{52}F_6N_8O_7OsP$ $[M]^+$ 1380.342, found 1382 $[M]^+$, 618 $[M]^{2+}$.

Phosphoramidite 7a. To a solution of **6a** (150 mg, 0.104 mmol) and (1*H*)-tetrazole (7 mg, 0.099 mmol) in 2 mL anhydrous acetonitrile was added 2-cyanoethyl-*N*,*N*,*N*′,*N*′-tetraisopropyl-diphosphoramidite (63 mg, 0.209 mmol). The reaction was stirred for 4 h at room temperature under argon atmosphere. The reaction mixture was diluted with cold 1% triethylamine/dichloromethane (300 mL), and washed with 1 M $NaHCO_3$ (2 × 20 mL) and brine (2 × 20 mL). The organic phase was dried over Na_2SO_4 and concentrated. The crude product was purified by flash chromatography (basic alumina, 0.5% saturated aqueous KPF_6, 2.5% water in acetonitrile). The product fractions were concentrated, dissolved in dichloromethane, and filtered to remove excess KPF_6. The product **7a** was obtained in 80% yield (136 mg) as a red foam. TLC (1% saturated aqueous KNO_3/10% HO/CH_3CN) R_f = 0.34; ^{1}H NMR (CD_3CN, 400 MHz): δ 8.60−8.63 (m, 1H), 8.49−8.54 (m, 3H), 8.45 (d, J = 6.8 Hz, 0.5H), 8.41 (t, J = 7.3 Hz, 1H), 8.33 (d, J = 6.8 Hz, 0.5H), 8.24 (d, J = 9.4 Hz, 0.5H), 8.21 (d, J = 9.4 Hz, 0.5H), 7.96−8.12 (m, 6H), 7.90 (d, J = 9.3 Hz. 0.5H), 7.86 (d, J = 5.4 Hz), 7.72−7.82 (m, 3H), 7.50−7.57 (m, 2H), 7.25−7.46 (m, 10H), 7.20 (t, J = 6.8 Hz, 0.5H), 7.13 (t, J = 7.8 Hz, 1H), 7.07 (t, J = 7.3 Hz, 1H), 6.98 (t, J = 6.8 Hz, 0.5H), 6.82 (d, J = 8.8 Hz, 1H), 6.72−6.80 (m, 2H), 6.61 (d, J = 8.3 Hz, 1H), 6.14−6.19 (m, 1H, H-1′), 4.72−4.76 and 4.67−4.71 (m, 1H, H-3′), 4.09−4.20 (m, 1H, H-4′), 3.18−3.83 (m, 12H, -NCH(CH_3)$_2$, −OCH_2CH$_2$CN, OCH_3, H-5′), 2.63−2.66 and 2.50−2.54 (m, 2H, -OCH$_2$CH_2CN), 2.47−2.58 (m, 2H, H-2′), 1.13−1.19 (m, 9H, -NCH(CH_3)$_2$), 1.08 and 1.04 (d, J = 6.8 Hz, 3H, -NCH(CH_3)$_2$; ^{31}P NMR (CD_3CN, 269 MHz) δ 292.69, 292.62, 292.54 (m); ESI MS calcd for $C_{73}H_{69}F_6N_{10}O_8P_2Ru$ $[M]^+$ 1491.339, found 1492 $[M]^+$, 673 $[M]^{2+}$.

Phosphoramidite Λ-7a. The red foam Λ-**7a** was obtained by the same procedure described above for phosphoramidite **7a** from compound Λ-**6a** in 90% yield. TLC (1% saturated aqueous KNO_3/10% H_2O/CH_3CN) R_f = 0.34; ^{1}H NMR (CD_3CN, 400 MHz): δ 8.59 (d, J = 7.8 Hz, 1H), 8.43−8.52 (m, 5H), 8.19 (d, J = 8.8 Hz, 1H), 7.93−8.10 (m, 6H), 7.84 (d, J = 5.9 Hz, 1H), 7.70−7.77 (m, 3H), 7.49 (d, J = 5.9 Hz, 2H), 7.16−7.45 (m, 11H), 7.04 (t, J = 7.8 Hz, 2H), 6.80 (d, J = 8.8 Hz, 2H), 6.71−6.76 (m, 3H), 6.14 and 6.16 (t, J = 5.9 Hz, 1H, H-1′), 4.62−4.68 (m, 1H, H-3′), 4.12−4.18 (m, 1H, H-4′), 3.10−3.80 (m, 12H, -NCH(CH_3)$_2$, −OCH_2CH$_2$CN, −OCH$_3$, H-5′), 2.63 and 2.50 (t, J = 5.9 Hz, 2H, −OCH$_2$CH_2CN), 2.43−2.55 (m, 2H, H-2′), 1.12−1.16 (m, 9H, -NCH(CH_3)$_2$), 1.03 (d, J = 6.8 Hz, 3H, -NCH-(CH_3)$_2$); ^{31}P NMR (CD_3CN, 269 MHz) δ 292.57, 292.46; ESI MS calcd for $C_{73}H_{69}F_6N_{10}O_8P_2Ru$ $[M]^+$ 1491.339, found 1492 $[M]^+$, 673 $[M]^{2+}$.

Phosphoramidite Δ-7a. Product Δ-**7a** was obtained in 68% yield as described above for phosphoramidite **7a**. TLC (1% saturated aqueous KNO_3/10% H_2O/CH_3CN) R_f = 0.34; ^{1}H NMR (CD_3CN, 400 MHz): δ 8.61 (d, J = 7.3 Hz, 1H), 8.50 (d, J = 7.8 Hz, 1H), 8.47 (d, J = 7.8 Hz, 1H), 8.39 (t, J = 7.8 Hz, 2H), 8.32 (d, J = 6.4 Hz, 1H), 8.23 (d, J = 9.3 Hz, 1H), 8.08 (t, J = 8.3 Hz, 1H), 7.94−8.04 (m, 5H), 7.90 (d, J = 8.8 Hz, 1H), 7.79 (d, J = 5.4 Hz, 1H), 7.70−7.74 (m, 2H), 7.56 (d, J = 5.9 Hz, 1H), 7.52 (d, J = 5.4 Hz, 1H), 7.41−7.45 (m, 3H), 7.33−7.39 (m, 4H), 7.23−7.30 (m, 4H), 7.11 (t, J = 7.8 Hz, 2H), 6.95−6.98 (m, 1H), 6.71 (d, J = 7.8 Hz, 2H), 6.58 (d, J = 8.8 Hz, 2H), 6.13 and 6.15 (t, J = 6.4 Hz, 1H, H-1′), 4.70−4.76 (m, 1H, H-3′), 4.07−4.13 (m, 1H, H-4′), 3.31−3.83 (m, 12H, -NCH(CH_3)$_2$, -OCH_2-CH$_2$CN, −OCH$_3$, H-5′), 2.64−2.67 and 2.49−2.51 (t, J = 5.9 Hz, 2H, -OCH$_2$CH_2CN), 2.54 (t, J = 5.9 Hz, 2H, H-2′), 1.15−1.21 (m, 9H, -NCH(CH_3)$_2$), 1.08 (d, J = 6.8 Hz, 3H, -NCH(CH_3)$_2$); ^{31}P NMR (CD_3-CN, 269 MHz) δ 292.50, 292.45, 292.39; ESI MS calcd for $C_{73}H_{69}F_6N_{10}O_8P_2Ru$ $[M]^+$ 1491.339, found 1492 $[M]^+$, 673 $[M]^{2+}$.

Phosphoramidite 7b. The dark brown foam **7b** was obtained in 84% yield from **6b** by the same procedure described above for phosphoramidite **7a**. TLC (1% saturated aqueous KNO_3/10% H_2O/CH_3-CN) R_f = 0.35; ^{1}H NMR (CD_3CN, 400 MHz): δ 8.42−8.50 (m, 3.5H), 8.35−8.40 (m, 2H), 8.30 (d, J = 5.1 Hz, 0.5H), 8.21 (d, J = 9.2 Hz, 0.5H), 8.19 (d, J = 8.8 Hz, 0.5H), 7.95−7.97 (m, 1H), 7.85−7.92 (m, 3H), 7.75−7.73 (m, 3.5H), 7.70 (d, J = 5.9 Hz, 0.5H), 7.63−7.67 (m, 1.5H), 7.60 (d, J = 5.5 Hz, 0.5H), 7.26−7.45 (m, 10.5H), 7.00−7.17 (m, 5H), 6.80 (d, J = 8.8 Hz, 1H), 6.70−6.78 (m, 2.5H), 6.59 (d, J = 8.8 Hz, 1H), 6.11−6.17 (m, 1H, H-1′), 4.65−4.76 (m, 1H, H-3′), 4.07−4.19 (m, 1H, H-4′), 3.16−3.83 (m, 4H, -NCH(CH_3)$_2$, -OCH_2CH$_2$CN), 3.59 (d, J = 1.1 Hz, 1.5H, -OCH_3), 3.57 (d, J = 1.8 Hz, 1.5H, -OCH_3), 3.55 (d, J = 4.0 Hz, 1.5H, −OCH_3), 3.48 (s, 1.5H, -OCH_3), 3.31−3.34 (m, 1H, H-5′$_A$), 3.18 (dt, J = 11.0, 2.9 Hz, 1H, H-5′$_B$), 2.62−2.67 and 2.52−2.55(m, 2H, -OCH$_2$CH_2CN), 2.42−2.58 (m, 2H, H-2′),

1.12−1.20 (m, 9H, -NCH(CH_3)$_2$), 1.08 (d, J = 6.7 Hz, 1.5H, -NCH(CH_3)$_2$), 1.04 (d, J = 6.8 Hz, 1.5H, -NCH(CH_3)$_2$); ^{31}P NMR (CD_3CN, 202 MHz) δ 292.34 (m); ESI MS calcd for $C_{73}H_{69}F_6N_{10}O_8OsP_2$ $[M]^+$ 1580.559, found 1581 $[M]^+$, 717 $[M]^{2+}$.

[(bpy)$_2$Ru(3-phenylethynyl-1,10-phenanthroline)]$^{2+}$ 8. Ru^{II} complex **4a**[13] (50 mg, 0.052 mmol), Pd(dppf)Cl_2·CH_2Cl_2 (2.4 mg, 0.003 mmol), and CuI (1.0 mg, 0.003 mmol) were dissolved in a degassed solution of anhydrous DMF (3.0 mL), triethylamine (500 μL), and phenylacetylene (53 mg, 0.52) under argon. The solution was stirred under argon for 20 min at room temperature, then evaporated under reduced pressure. The crude reaction mixture was purified by flash chromatography (silica gel, 0.2% saturated aqueous KNO_3, 5% water in acetonitrile). The product fractions were concentrated, dissolved in Milli-Q water, and extracted into dichloromethane after the addition of excess KPF_6. The product solution was dried over Na_2SO_4, filtered, and evaporated to dryness to yield product **8** in 94% yield (48 mg). TLC (1% saturated aqueous KNO_3/10% H_2O/CH_3CN) R_f = 0.25; ^{1}H NMR (CD_3CN, 400 MHz): δ 8.74 (d, J = 1.5 Hz, 1H), 8.62 (dd, J = 8.4, 1.1 Hz, 1H), 8.49−8.56 (m, 3H), 8.28 (d, J = 8.8 Hz, 1H), 8.23 (d, J = 8.8 Hz, 1H), 8.22 (d, J = 1.8 Hz, 1H), 8.08−8.12 (m, 3H), 7.99−8.04 (m, 2H), 7.87 (d, J = 5.1 Hz, 1H), 7.82 (d, J = 5.5 Hz, 1H), 7.75 (dd, J = 8.1, 5.1 Hz, 1H), 7.66 (d, J = 5.1 Hz, 1H), 7.52−7.56 (m, 3H), 7.42−7.48 (m, 5H), 7.22−7.27 (m, 2H); ^{13}C NMR (CD_3CN, 101 MHz): δ 85.32, 96.14, 122.19, 123.05, 125.03, 125.11, 125.16, 125.21, 127.11, 128.24, 128.28, 128.45, 128.59, 129.73, 130.72, 131.20, 132.23, 132.53, 137.73, 138.65, 138.78, 139.50, 147.17, 148.16, 152.73, 152.77, 152.94, 153.01, 153.67, 154.68, 157.73, 157.87, 158.06, 158.08; UV (CH_3CN): λ_{max} nm ($\epsilon \times 10^{-4}$) 242 (4.0), 286 (7.5), 332 (2.7), 450 (1.3); ESI MS calcd for $C_{40}H_{28}F_6N_6PRu$ $[M]^+$ 838.72, found 838.8 $[M]^+$.

Oligonucleotide Synthesis. All oligonucleotides were prepared on a 0.2 μmol scale on 500-Å CPG solid support using a Milligen Cyclone Plus DNA synthesizer. Metal modified residues were introduced site-specifically by trityl-off synthesis of the base oligonucleotide, followed by the manual coupling of the desired metal-modified phosphoramidite. In a typical procedure, the modified nucleoside (0.02 mmol) is dissolved in 200 μL of 0.5 M (1*H*)-tetrazole in acetonitrile. This activated phosphoramidite solution is immediately applied via syringe to the synthesis column containing the CPG-bound base oligonucleotide. Coupling times for the modified phosphoramidites were extended to 5 min to ensure maximum coupling efficiency. The column was rinsed with dry acetonitrile (5 mL), and returned to the automated synthesizer for the standard oxidation and capping steps. Coupling efficiencies for the base-modified phosphoramidites as monitored by trityl cation assay were consistently above 90%. Shorter coupling times and/or less concentrated (1*H*)-tetrazole yielded significantly lower coupling efficiency, ranging from 25 to 40%. The remainder of the desired oligonucleotide was synthesized normally using the trityl-off procedure. The oligonucleotide was cleaved from the solid support by treatment with 1.0 mL of 30% aqueous ammonium hydroxide for 3 h at room temperature. The resulting solution was incubated at 55 °C for 8 h. Oligonucleotides containing no modified bases were synthesized using standard Milligen/Biosearch Cyclone Plus protocols. The crude product from the automated oligonucleotide synthesis was lyophilized and purified by preparative 20% denaturing polyacrylamide gel electrophoresis. The product was visualized by UV shadowing, and the desired band excised from the gel. The band was crushed, then extracted with 1× TBE buffer pH 8.3 (90 mM Tris, 90 mM boric acid, 1 mM EDTA) for 24−36 h. The extract was filtered (0.45 μm nylon), and desalted using a Sep-pak cartridge (Waters Corporation, MA). Oligonucleotides were eluted from the Sep-pak cartridge using 40% acetonitrile/water. The concentration of the single-stranded oligonucleotides was determined at 260 nm using the following molar extinction coefficients: 15400 (A), 11700 (G), 8800 (T), 7300 (C), 36500 (U^{Ru}), 33200 (U^{Os}). This procedure assumes that the absorption properties of the free 5-modified 2′-deoxyuridine nucleosides remain unchanged upon incorporation into single stranded DNA. 8-mer oligonucleotides (**10**−**13**) were purified by reverse-phase HPLC following gel purification using the following conditions: Vydac C-8 analytical column, 4.6 × 250 mm, 5μ, 1−12% CH_3CN in 50 mM triethylammonium acetate, pH 7.0 over 12 min, with a gradient to 50% CH_3CN over the next 30 min. The retention time of the metal-modified 8-mer oligonucleotides was approximately 12 min.

Crude metal-containing oligonucleotides were alternatively purified by trityl-on reverse phase HPLC. The finished oligonucleotide was cleaved from the solid support, and the exocyclic amines were deprotected by treatment with 1.0 mL of 30% aqueous ammonium hydroxide for 24 h at room temperature. The solution was lyophilized, and the crude oligonucleotide was purified using semi-prep HPLC (Vydac C-8 column, 10 × 250 mm, 5μ, 300 Å pore size). HPLC mobile phase: 20−25% acetonitrile gradient in 50 mM triethylammonium acetate pH 7.0 over 30 min. Trityl-on metalated oligonucleotides typically eluted between 12 and 20 min depending on length, and were lyophilized immediately after collection. The purified oligonucleotide was then treated with 0.5 mL of 80% acetic acid at room temperature for 20 min. The solution was lyophilized, dissolved in 1× TBE buffer pH 8.3, and applied to a Sep-pak cartridge. The oligonucleotide was desalted and eluted using 20% CH_3CN/H_2O. Quantification of the HPLC purified oligonucleotides was performed as above.

Enzymatic Degradation of Oligonucleotides. The general procedure is as follows: To a 2-nmol pellet of DNA were added 10 μL of 1 M $MgCl_2$, 10 μL of 10× AP buffer (New England Biolabs), 2 μL (0.3 U/μL) of nuclease P1 (Boehringer Mannheim), 1.5 μL (0.003 U/μL) of snake venom phosphodiesterase (Boehringer Mannheim), 1.5 μL (10 U/μL) of alkaline phosphatase (New England Biolabs), and 75 μL of water. The reaction mixture was incubated at 37 °C for 6 h, passed through a 0.45 μm Nylon-66 micro-centrifuge filter (Rainin), and analyzed by HPLC (Vydac C18 column, 4.6 × 250 mm, 5μ RP-silica) using a photodiode array detector with detection at 260, 358, and 450 nm. HPLC mobile phase: 1−12% acetonitrile gradient in 100 mM triethylammonium acetate pH 5.5 over 12 min, followed by 12−99% acetonitrile gradient over 30 min. Peaks were identified by retention time and UV spectra, as well as by comparison with authentic standards. Nucleoside ratios were determined by integration of peak areas at 260 nm and normalization using the extinction coefficients listed above. Enzymatic digestion performed with snake venom phosphodiesterase and alkaline phosphatase resulted in incomplete digestion and termination at the nonnatural base. The endonuclease nuclease P1 is required for complete degradation of these metal modified oligonucleotides to their constituent nucleosides.[23]

Circular Dichroism. CD spectra were collected on an Aviv model 202 spectropolarimeter at 25 °C in a 1-cm path length cell at 1-nm intervals using a 4 s averaging time. The concentrations of metal-modified nucleosides were 2 × 10^{-5} M in spectral grade acetonitrile. The concentrations of DNA duplexes were 1 μM in 100 mM NaCl, 10 mM phosphate, pH 7.0.

Thermal Denaturation Studies. All hybridizations and UV melting experiments were carried out in 100 mM NaCl, 10 mM phosphate buffer, pH 7.0 containing a one-to-one ratio of complementary oligonucleotides at 2 μM duplex concentration. After samples were prepared, they were heated to 90 °C for 5 min, cooled to room temperature for 2−3 h, then cooled to 4 °C prior to melting temperature (T_m) measurement. Thermal denaturation studies were carried out in a Teflon-stoppered 1.0-cm path length quartz cell on a Varian-Cary 1E spectrophotometer with a temperature-controlled cell compartment. Samples were equilibrated at the starting temperature for 20 min. Heating runs were performed between 50 and 90 °C at a scan rate of 0.5 °C min^{-1} with optical monitoring at 260 nm. All duplexes displayed sharp, two-state transition curves from duplex to single-stranded DNA. Similar results were seen in cooling curves. T_m values were determined by computer fit of the melting data, followed by calculation of the

first derivative of the resulting melting curve. Uncertainty in T_m values is estimated to be ± 0.5 °C.

Steady-State Luminescence Experiments. Steady-state luminescence experiments were conducted at 20 °C with excitation at 450 nm on a Perkin-Elmer LS 50B luminescence spectrophotometer. Argon-degassed samples were measured at a duplex concentration of 2 μM in 100 mM NaCl, 10 mM sodium phosphate buffer at pH 7.0. Quenching efficiencies were determined by integration of the emission curves obtained from duplicated experiments on two separately prepared samples.

Time-Resolved Emission Spectroscopy. The excited-state lifetimes of the emissive complexes were measured using the same samples used for the steady-state luminescence studies. The degassed solutions were excited by a 4-ns pulsed dye-laser. The laser was tuned to 450 nm for measurement of free nucleosides and singly metal-modified strands and duplexes. For duplexes containing both Os^{II}- and Ru^{II}-modified nucleotides, the laser was tuned to 467 nm. At this wavelength, the ratio of the extinction coefficients for the Ru^{II} nucleoside **5a** and the Os^{II} nucleoside **5b** is 1.0. The emitted light was collected at 90° and focused into a monochromator. Detection was achieved by a photomultiplier tube connected to a LeCroy Digitizing oscilloscope. The data from the scope was transferred to a PC and processed by using routine software of local origin. A sample of $[Ru(bpy)_3](PF_6)_2$ in acetonitrile was measured before and after each set of data acquisition to ensure the stability and accuracy of the setup.

Acknowledgment. We thank the National Institutes of Health (GM 58447) for supporting this research and Clinical Micro Sensors, Inc., and the UC Biotechnology STAR Project for supporting the early stages of the project. We are grateful to Professor Doug Magde (UCSD) for his help and insightful comments regarding the time-resolved luminescence measurements. We thank Susan Seaman and Edith (Phoebe) Glazer for assistance with electrochemical measurements and Dr. Natia Frank for her help with measuring transient absorption spectra.

Supporting Information Available: Additional data regarding solvatochromism studies, determination of the excited-state localization and redox potential, as well as thermal denaturation measurements, HPLC and enzymatic digestions of metalated oligonucleotides, and synthesis and NMR spectroscopy of diastereomerically pure metalated nucleosides (PDF). This material is available free of charge via the Internet at http://pubs.acs.org.

JA0123103